The Company of Biologists

RESEARCH ARTICLE

Opposing effects of an F-box protein and the HSP90 chaperone network on microtubule stability and neurite growth in *Caenorhabditis elegans*

Chaogu Zheng[1,2,*], Emily Atlas[2], Ho Ming Terence Lee[1], Susan Laura Javier Jao[2], Ken C. Q. Nguyen[3], David H. Hall[3] and Martin Chalfie[2,*]

ABSTRACT

Molecular chaperones often work collaboratively with the ubiquitylation-proteasome system (UPS) to facilitate the degradation of misfolded proteins, which typically safeguards cellular differentiation and protects cells from stress. In this study, however, we report that the Hsp70/Hsp90 chaperone machinery and an F-box protein, MEC-15, have opposing effects on neuronal differentiation, and that the chaperones negatively regulate neuronal morphogenesis and functions. Using the touch receptor neurons (TRNs) of *Caenorhabditis elegans*, we find that *mec-15(-)* mutants display defects in microtubule formation, neurite growth, synaptic development and neuronal functions, and that these defects can be rescued by the loss of Hsp70/Hsp90 chaperones and co-chaperones. MEC-15 probably functions in a Skp-, Cullin- and F-box-containing complex to degrade DLK-1, which is an Hsp90 client protein stabilized by the chaperones. The abundance of DLK-1, and likely other Hsp90 substrates, is fine-tuned by the antagonism between MEC-15 and the chaperones; this antagonism regulates TRN development, as well as synaptic functions of GABAergic motor neurons. Therefore, a balance between the UPS and the chaperones tightly controls neuronal differentiation.

KEY WORDS: Neurite growth, Microtubules, Molecular chaperones, Ubiquitylation-proteasome system, Protein homeostasis, Touch receptor neurons

INTRODUCTION

Molecular chaperones, including the heat shock proteins (Hsps), play essential roles in protein maturation, refolding and degradation (Hartl et al., 2011; Lindquist and Craig, 1988). Although the function of Hsps in the response to stress has been extensively characterized, their roles in neuronal differentiation are much less well understood. Ishimoto et al. (1998) found that Hsp90 promotes neurite extension for the chick telencephalic neurons and spinal neurons *in vitro*. More recently, pharmacological inhibition of Hsp90 by 17-demethoxygeldanamycin (17-AAG) disturbed neuronal polarization and axonal elongation of cultured hippocampal neurons (Benitez et al., 2014). Hsp90 inhibition

decreased the expression of two Hsp90 client proteins, Akt and GSK3, which have diverse functions in cell differentiation. Thus, Hsp90 might regulate axon specification and growth by affecting specific signaling pathways through its chaperone activity. Given that the Hsp70 and Hsp90 chaperones interact with numerous client proteins, including transcription factors, kinases and signaling molecules (Wayne et al., 2011), the regulation of neuronal morphogenesis by the chaperones is probably context dependent. However, whether Hsp70 and Hsp90 chaperones, and their co-chaperones, can also negatively regulate neurite growth is unclear.

The ubiquitylation-proteasome system (UPS) often works in concert with the chaperone-mediated refolding machinery for protein quality control, which promotes the degradation of numerous misfolded proteins in a chaperone-dependent manner (Buchberger et al., 2010). In developing neurons, this process safeguards the protein quality of important guidance molecules. For example, in *Caenorhabditis elegans* the BC-box protein EBAX-1, the substrate-recognition subunit of the Elongin BC-containing Cullin-RING ubiquitin ligase (CRL) and HSP-90/Hsp90 collaboratively regulate the folding and degradation of misfolded SAX-3/Robo receptor during axonal pathfinding (Wang et al., 2013). By preferentially binding to misfolded SAX-3, EBAX-1 not only recruits Hsp90 to promote the refolding of non-native SAX-3 but also mediates the degradation of irreparable SAX-3 through CRL activity.

Despite known examples of collaboration, the UPS and molecular chaperones could theoretically also have opposing effects, as the UPS increases normal protein turnover and chaperones can enhance protein stability. The antagonism of the UPS and the molecular chaperone machinery during neuronal differentiation, however, has not, to our knowledge, been previously reported.

In this study, we found that the F-box and WD40 repeat domain-containing protein MEC-15 (an ortholog of human FBXW9), and ubiquitylation, promoted microtubule (MT) stability and neurite growth by countering the activity of the Hsp70/Hsp90 chaperone network. Mutations in *mec-15* led to a range of developmental defects in the *C. elegans* touch receptor neurons (TRNs), including the loss of MTs, inhibited neurite growth and branching, defects in localizing synaptic proteins, and the loss of sensory function. All of these defects in *mec-15* mutants could be rescued by removing the Hsp70 and Hsp90 chaperones and co-chaperones, which unexpectedly suggests that the chaperones can disrupt neurite growth and neuronal development, and that this activity is normally suppressed by the F-box protein and the ubiquitylation pathway. Downstream of the chaperones, we identified the MAP3 kinase DLK-1 as an Hsp90 client protein that has MT-destabilizing activity and can inhibit neurite growth. Therefore, our studies provide an important example of how the effects of molecular

[1]School of Biological Sciences, The University of Hong Kong, Hong Kong SAR, China. [2]Department of Biological Sciences, Columbia University, New York, NY 10027, USA. [3]Department of Neuroscience, Albert Einstein College of Medicine, Bronx, NY 10461, USA.

*Authors for correspondence (cgzheng@hku.hk; mc21@columbia.edu)

C.Z., 0000-0002-5048-4520; E.A., 0000-0002-0705-6109; M.C., 0000-0002-9079-7046

DEVELOPMENT

chaperones are opposed by the ubiquitylation pathway during neuronal differentiation.

RESULTS

The F-box protein MEC-15 is required for MT stability and neurite growth

The six *C. elegans* touch receptor neurons (ALML/R, PLML/R, AVM and PVM) are mechanosensory neurons that respond to gentle touch and have a simple morphology (Fig. 1A,B). We previously identified a set of neomorphic tubulin mutations that caused the formation of hyperstable MTs and the growth of an ectopic, posteriorly directed neurite in ALM neurons (termed ALM-PN; similarly, ALM-AN is the anteriorly directed neurite of ALM; PLM-AN and PLM-PN are the anteriorly and posteriorly directed neurites of PLM, respectively; Zheng et al., 2017). Among those mutants, the β-tubulin *mec-7(u278; C303Y)* allele had the strongest phenotype, with a very long ALM-PN extending to the tail region. By suppressing this *mec-7(neo)* phenotype, we sought to identify genes

that regulate MT stability and neurite development. This *mec-7(u278)* suppressor screen (see Materials and Methods) yielded a *mec-15* nonsense allele *u1042(*R26**)* that completely suppressed the growth of ALM-PN in *mec-7(u278)* mutants. Another *mec-15* loss-of-function (*lf*) allele *u75(*Q118**)* showed similar suppression (Fig. 1A,B; Fig. 2A). *mec-15* codes for a protein that contains an N-terminal F-box and four WD40 repeats (Fig. 1C; Bounoutas et al., 2009b), and is orthologous to human FBXW9.

The loss of *mec-15* also suppressed the growth of ectopic ALM-PN induced by other mutations that increased MT stability and caused the formation of an ALM-PN (Fig. 1D), including another neomorphic β-tubulin mutation *mec-7(u1017; L377F)*, an *lf* mutation in a destabilizing α-tubulin gene *tba-7* and an *lf* mutation in a MT-depolymerizing kinesin-13 gene *klp-7* (Zheng et al., 2017). These data suggest that MEC-15, an F-box protein, is generally required for the excessive neurite growth triggered by elevated MT stability in TRNs.

MEC-15 is also required for normal TRN morphology. *mec-15(lf)* alleles *u75* and *u1042* caused the shortening of both
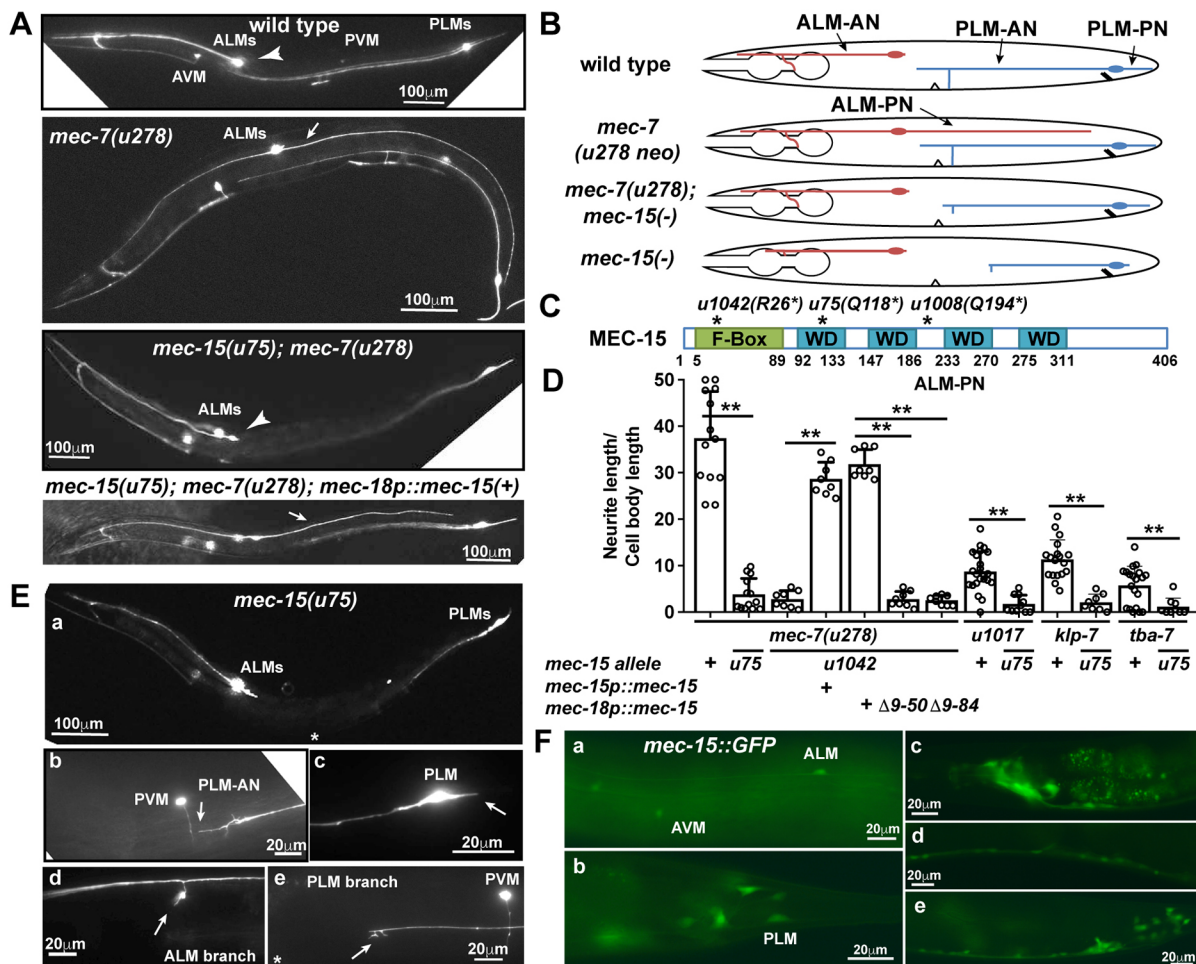

Fig. 1. F-box protein MEC-15 promotes neurite growth. (A) The ALM-PN is missing in the wild-type animals (arrowhead) but is extensive (arrow) in *mec-7(u278 neo)* mutants. *mec-15 lf* mutations suppressed ALM-PN production in *mec-7(u278)* mutants but the ALM-PN can be restored in the double mutants by expressing wild-type MEC-15 under a TRN-specific *mec-18* promoter. (B) Schematic representation of ALM and PLM morphologies (with labeled neurites) in wild-type and mutant animals. (C) Protein structures of the wild-type MEC-15 with the F-box and the four WD40 repeats (WD) labeled in green and blue, respectively. Numbers indicate amino acid positions. (D) The normalized length (mean±s.d.) of ALM-PN in various strains. Here, and in all other figures, data are mean±s.d., with individual data points indicated and asterisks indicate significant difference (*P<0.05 and **P<0.01) in ANOVA and Tukey–Kramer test. (E) TRN morphology in *mec-15(u75 lf)* mutants. (Ea) low magnification view. (Eb) PLM-AN (arrow) was shortened and did not extend beyond PVM. (Ec) PLM-PN (arrow) was also significantly shortened. Synaptic branches (arrow) of (Ed) ALM-AN and (Ee) PLM-AN could not fully extend in *mec-15* mutants. (F) The expression of *mec-15::GFP* in (Fa) anterior and (Fb) posterior TRNs, (Fc) head neurons, (Fd) ventral cord neurons, and (Fe) the pre-anal ganglion and the tail. Scale bars: 100 μm in A,Ea; 20 μm in Eb-e,F.
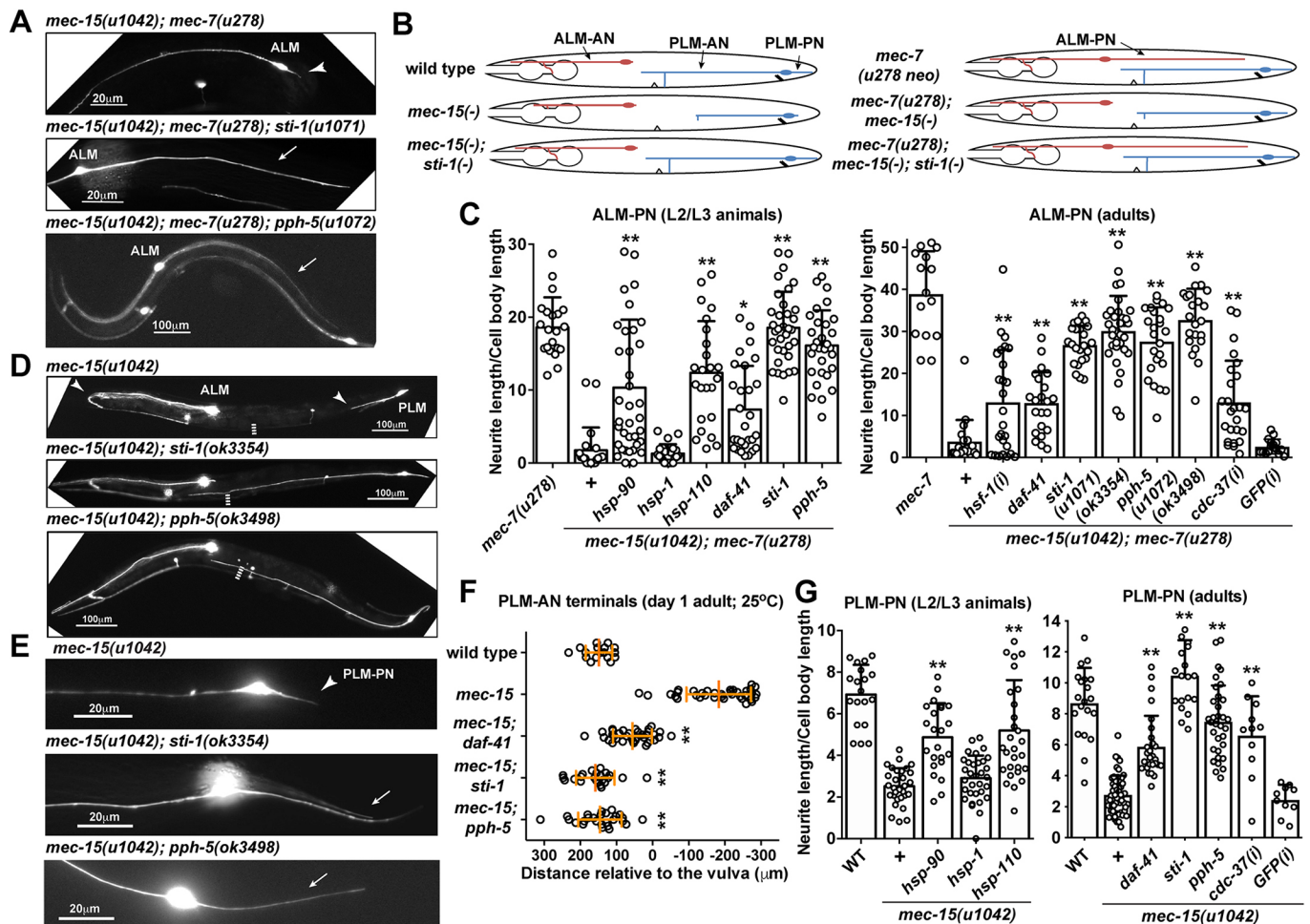
Fig. 2. Loss of Hsp90 chaperones suppress the neurite growth defects in *mec-15 lf* mutants. (A) ALM-PN is absent in *mec-15; mec-7* mutants (arrowhead) and restored in *mec-15; mec-7; sti-1* and *mec-15; mec-7; pph-5* triple mutants (arrows). (B) Schematic representation of ALM and PLM morphologies in wild-type and various mutants. *sti-1(−)* is used as an example of *mec-15(−)* suppressors. (C) The length of ALM-PN in various mutants. *hsp-90(ok1333)*, *hsp-1(ok1371)* and *hsp-110(gk533)* alleles caused larval arrest and were examined at L2/L3 stages. *daf-41(ok3052)*, *sti-1(u1071)* and *pph-5(u1072)* were examined at both L2/L3 and adult stages; *sti-1(ok3354)* and *pph-5(ok3498)* deletion alleles served as references. *mec-15; mec-7* adult animals carrying transgenes expressing dsRNA against *hsf-1* or *cdc-37* in TRNs were examined; results are labeled as *hsf-1(i)* and *cdc-37(i)*, respectively. (D) Premature termination of ALM-AN and PLM-AN (arrowheads) in *mec-15* single mutants was rescued in *mec-15; sti-1* and *mec-15; pph-5* double mutants. Dashed line indicates the position of the vulva. (E) Shortening of PLM-PN (arrowhead) in *mec-15* single mutants was rescued to its normal length (arrows) in the double mutants. (F) The anterior extent of PLM-AN growth in 1-day-old adults of various mutants grown at 25°C. Distances are given relative to the position of the vulva, so positive values indicate that the PLM-AN grew past the vulva towards the anterior. (G) PLM-PN length in wild type (WT) and various mutants. For F and G, *daf-41(ok3052)*, *sti-1(u1071)*, *pph-5(u1072)*, *hsp-1(ok1371)*, *hsp-90(ok1333)* and *hsp-110(gk533)* were examined. Asterisks indicate statistical significance for the difference between the *mec-7; mec-15* and the triple mutants (C) or between the *mec-15* and the double mutants (G) in ANOVA and Tukey–Kramer test. Data are mean±s.d. (*$P<0.05$ and **$P<0.01$).

PLM-AN and PLM-PN in an otherwise wild-type background (Fig. 1E; Fig. 2D; Fig. S1). Another *mec-15* nonsense allele *u1008(*Q194*)*, isolated from a different screen (Zheng et al., 2017), showed similar TRN morphological defects (Fig. S1A-C). Previous studies found that *mec-15* is required for touch sensitivity and the localization of presynaptic proteins in TRNs (Bounoutas et al., 2009b). We found that the ALM-AN and PLM-AN in *mec-15* mutants could not fully extend their synaptic branches (Fig. 1 Ed,Ee), which might have caused the synaptic defects.

As previously found (Bounoutas et al., 2009b; Sun et al., 2013), a *mec-15::GFP* translational reporter was expressed in the TRNs, several head and tail neurons, and ventral cord motor neurons (Fig. 1F). We also generated a *mec-15::GFP* knock-in allele at the endogenous *mec-15* locus through CRISPR/Cas9-mediated gene editing, but the resulting strain did not have any detectable GFP expression, suggesting that the endogenous MEC-15 level might

be quite low. We next tested whether MEC-15 functions cell-autonomously in the TRNs. Expression of wild-type *mec-15(+)* from the TRN-specific *mec-18* promoter rescued both the neurite growth defects in *mec-15(−)* single mutants and the loss of ALM-PN in *mec-15(−); mec-7(u278 neo)* double mutants. In contrast, the expression of MEC-15 with some or all of the F-box domain removed, could not rescue either phenotype (Fig. 1D; Fig. S1A-C), suggesting that MEC-15 functions within the TRNs and its activity requires the F-box domain.

F-box proteins assemble with Skp and Cullin proteins to form Skp, Cullin, F-box containing complex (SCF) E3 ubiquitin ligase complexes. The involvement of ubiquitylation in the action of MEC-15 was supported by the finding that TRN-specific knockdown of *uba-1*, the only known *C. elegans* gene encoding a ubiquitin-activating enzyme, strongly suppressed the growth of ALM-PN in *mec-7(u278 neo)* mutants (Fig. S1D). Because

mutation or general knockdown of *uba-1* causes sterility and lethality, we performed cell-specific RNAi by expressing double-stranded RNA (dsRNA) against *uba-1* using the TRN-specific *mec-17* promoter. As a negative control, expression of dsRNA against GFP did not affect neurite growth. Moreover, the inhibition of proteasomes by bortezomib partially suppressed the growth of ALM-PN (Fig. S1D). In addition, previous work found that MT depolymerization led to a general reduction in protein levels in TRNs (Bounoutas et al., 2011). We found that mutations in *mec-15*, knockdown of *uba-1* and bortezomib treatment all significantly reduced TagRFP expression from a *mec-17p::TagRFP* transgene in the TRNs, as measured by fluorescent intensity (Fig. S1E). The above data lead to the hypothesis that an MT-destabilizing molecule, which is normally ubiquitylated and targeted for degradation by MEC-15, accumulated abnormally in the *mec-15*-deficient TRNs, leading to reduced MT stability and the inhibition of neurite growth.

Although reduced *uba-1* activity affected ALM-PN outgrowth, we could not identify the other components of the putative SCF complex. In fact, our results suggest that these other components may be redundant. For example, although we found that MEC-15 physically interacted with the Skp homolog SKR-1 in a yeast two-hybrid assay (Fig. S1F), *skr-1(ok1696)* null mutations neither caused TRN morphological defects nor suppressed ALM-PN outgrowth in *mec-7(u278 neo)* mutants. In addition, RNAi of *skr-2*, *skr-8*, *skr-9*, *skr-12* and *skr-13* (other Skp homologs) did not suppress the Mec-7(neo) phenotype (see Materials and Methods for details). Cullin, the third component of the SCF complex, also appeared to be redundant, as mutations or knockdown of Cullin homologs *cul-1*, *cul-2*, *cul-4*, *cul-5* and *cul-6* did not induce the same defect as the loss of MEC-15.

Loss of molecular chaperones suppresses neurite growth defects of *mec-15* mutants

To identify the downstream target(s) of the MEC-15-dependent ubiquitylation pathway, we screened for suppressors of *mec-15* in the *mec-15(u1042); mec-7(u278)* background and identified the phenotype-causing mutations in eight mutants with restored ectopic ALM-PNs (Table S1; see Materials and Methods for details). Among those mutants were one recessive *lf* allele of *sti-1* and four recessive *lf* alleles of *pph-5*. *sti-1* encodes a homolog of the Sti1/Hop co-chaperone that physically links Hsp70 and Hsp90 through the tetratricopeptide repeat (TPR)-domain (Schmid et al., 2012), and *pph-5* encodes a homolog of protein phosphatase 5 (PP5), a TPR-domain containing serine/threonine phosphatase that binds to Hsp90 and activates its kinase clients (Vaughan et al., 2008). Deletion alleles of either gene [*sti-1(ok3354)* and *pph-5(ok3498)*] also induced the growth of ALM-PN in *mec-15(u1042); mec-7(u278)* animals (Fig. 2A-C; Table S1).

As STI-1 and PPH-5 are components of the molecular chaperone pathway, we tested other genes in the same pathway. The removal of *hsp-90* (a Hsp90 homolog) and *hsp-110* (a Hsp70 family member) but not *hsp-1* (another Hsp70 family protein) suppressed the loss of MEC-15. *hsp-90(ok1333)* and *hsp-110(gk533)* deletion alleles caused larval arrest, but the arrested *mec-15(u1042); hsp-90(ok1333); mec-7(u278)* and *mec-15(u1042); hsp-110(gk533); mec-7(u278)* triple mutants had long ALM-PNs (Fig. 2C).

Moreover, TRN-specific knockdown of *hsf-1*/heat shock transcription factor 1, which activates the expression of Hsps and functions upstream of HSP-90 and HSP-110 (Singh and Aballay, 2006), also induced the growth of ALM-PNs in *mec-15(u1042); mec-7(u278)* double mutants (Fig. 2C). PP5, the PPH-5 homolog,

dephosphorylates the co-chaperone Cdc37 in yeast and mammals, which is essential for the folding and maturation of Hsp90-dependent protein kinases (Vaughan et al., 2008; Wandinger et al., 2006). TRN-specific RNAi silencing of *cdc-37*, *C. elegans* Cdc37, promoted the growth of ALM-PN in *mec-15(−); mec-7(u278)* animals (Fig. 2C), suggesting that some Hsp90 kinase clients might be involved in the regulation of neurite growth.

Through a candidate RNAi screen of 27 Hsp70/Hsp90-related genes (Table S2), we found that knocking down *daf-41*, which encodes the Hsp90 co-chaperone PTGES3/p23, also restored the growth of ALM-PNs in *mec-15(u1042); mec-7(u278)* animals (Fig. S2C). A *daf-41* deletion allele, *ok3052*, produced the same phenotype (Fig. 2C). Thus, the disruption of the Hsp70/Hsp90 chaperone machinery by the deletion of Hsp70, Hsp90, p23, Sti1/Hop, PP5 or Cdc37 rescued the loss of the F-box protein MEC-15.

Importantly, the suppression of *mec-15* loss did not depend on the presence of *mec-7(u278 neo)*. We crossed *lf* alleles of *hsp-110*, *hsp-90*, *daf-41/p23*, *sti-1* and *pph-5* with *mec-15(u1042)* to create double mutants, and found that the shortening of PLM-PN in *mec-15* single mutants was suppressed in all double mutants (Fig. 2E,G). TRN-specific knockdown of *cdc-37* had similar effects (Fig. 2G). In addition, we found that the PLM-AN outgrowth defect (but not that of PLM-PN) in *mec-15* null mutants was more severe at 25°C than at 20°C (Fig. S2A,B), suggesting that the abnormally accumulated proteins might have higher expression or exert a stronger MT-destabilizing activity at higher temperatures. This more severe PLM-AN growth defect at 25°C was also suppressed in *mec-15*; *daf-41*, *mec-15*; *sti-1* and *mec-15*; *pph-5* double mutants; most PLM-ANs extended fully and grew beyond the vulva (Fig. 2F). We could not measure the length of PLM-AN in *mec-15*; *hsp-110* and *mec-15*; *hsp-90* adults because those double mutants arrested at early larval stages.

HSP-90 and the co-chaperones DAF-41, STI-1 and PPH-5 are expressed in most *C. elegans* cells (Gillan et al., 2009; Richie et al., 2011; Song et al., 2009), and we confirmed their expression in the TRNs (Fig. S3A-C). Moreover, we were able to rescue the loss of *daf-41*, *sti-1* and *pph-5* in their double mutants with *mec-15(u1042)*, and their triple mutants with *mec-15(u1042); mec-7(u278)* by expressing the wild-type co-chaperone gene from a TRN-specific *mec-17* promoter, indicating that the chaperone pathway genes function cell-autonomously in the TRNs (Fig. S3D).

Moreover, *hsp-110*, *hsp-90*, *daf-41*, *sti-1* and *pph-5* single mutants did not show any TRN morphological defects (Fig. S4), and *daf-41*, *sti-1* and *pph-5* single mutants did not cause touch insensitivity (Fig. 4G; we could not test *hsp-110* and *hsp-90* homozygous mutants, which are quite uncoordinated and unhealthy, and arrest at larval stages). These results suggest that their activities are not normally required for TRN differentiation and function. Nevertheless, an inhibitory role for these Hsp70/Hsp90 chaperones and co-chaperones on TRN differentiation is revealed when *mec-15* is lost, because the chaperone proteins were required for the disruption of TRN morphology and functions in *mec-15(−)* mutants.

An unexpected maternal effect of chaperone and co-chaperone mutants

Mutants of chaperones and co-chaperones had unexpected strong maternal effects in suppressing the Mec-15 phenotype. For example, although paternally derived *sti-1/+; mec-15; mec-7* heterozygotes had short or no ALM-PN, similar to *mec-15; mec-7* animals, heterozygotes produced by *sti-1; mec-15; mec-7* homozygous mothers showed long ALM-PN (Fig. S5A). This result suggested

that despite the presence of zygotic *sti-1(+)*, the lack of maternally deposited STI-1 mRNAs or proteins into the oocytes was sufficient to suppress the defects caused by *mec-15(−)* mutations. Consistent with the maternal effect, *sti-1; mec-15; mec-7* homozygotes produced by the *sti-1/+; mec-15; mec-7* heterozygous mother had very short ALM-PN, whereas homozygotes derived from the homozygous mother had long ALM-PN (Fig. S5C). Similar maternal effects, in terms of the suppression of PLM neurite growth defects, were observed with the *sti-1; mec-15* double mutants in the absence of the *mec-7(u278 neo)* background, for the suppression of PLM neurite growth defects (Fig. S5B).

To reconcile this maternal effect with the cell-autonomous rescue of *sti-1* mutants, we hypothesize that the expression of the endogenous *sti-1(+)* gene in TRNs might be at a low level or have a late onset, which causes a dependency on the maternal contributed protein. Overexpression of *sti-1(+)* from the *mec-17* promoter, a strong TRN-specific promoter that is activated shortly after the generation of TRNs, might overcome the lack of maternally deposited STI-1.

Mutations in *pph-5* and *daf-41/p23* had similar maternal effects in either the *mec-15; mec-7* double mutants or the *mec-15* single mutants (Fig. S5A-C). Although *hsp-110(gk533)* homozygous deletion mutants arrested at early larval stages, a few in each generation escaped, became vulvaless adults and produced ~20 progeny. The *hsp-110; mec-15; mec-7* triple mutants derived from homozygous mothers had a longer ALM-PN than the ones derived from the *hsp-110/nT2; mec-15; mec-7* heterozygous mothers; *hsp-110; mec-15* double mutants produced by homozygous mothers also had a longer PLM-PN than the ones produced by the

heterozygous mothers (Fig. S5D,E). Thus, mutations in *hsp-110* (Hsp70) also showed maternal effects. We could not test the *hsp-90* mutants for maternal effects because no escapers were found.

Overall, our results suggest that maternally deposited chaperone and co-chaperone mRNAs or proteins have long-lasting effects on the regulation of neurite morphogenesis in terminally differentiated TRN neurons. This observation is quite surprising, given that the generation of those neurons occurs more than 7 h after fertilization at 20°C and requires 10 (for ALMs) or 12 (for PLMs) rounds of embryonic cell divisions from the zygote (Sulston et al., 1983), and that neurite extension continuously occurs for three days in post-embryonic development after hatching.

Phosphorylation of STI-1 inhibits its activity in regulating neurite growth

Because mutations in *pph-5* and *sti-1* showed the strongest and almost identical effects in suppressing the *mec-15(−)* phenotype, we speculated whether, in addition to activating Hsp90 and Cdc37, PPH-5 might also activate STI-1 activity through dephosphorylation. This hypothesis is based on previous findings that the phosphorylation of yeast Sti1 and human Hop, which are STI-1 homologs, appeared to inhibit their co-chaperone activity (Röhl et al., 2015).

Both yeast and human Sti1/Hop proteins contain three TPR domains and two DP (aspartate and proline rich) domains; the TPR2A domain interacts with Hsp90, whereas the TPR1 and TPR2B domains interact with Hsp70 (Schmid et al., 2012). Although *C. elegans* STI-1 contains only TPR2A and TPR2B, and one DP domain (Fig. 3A), STI-1 is probably capable of transferring clients from Hsp70 and Hsp90. Yeast and human Sti1/Hop proteins contain
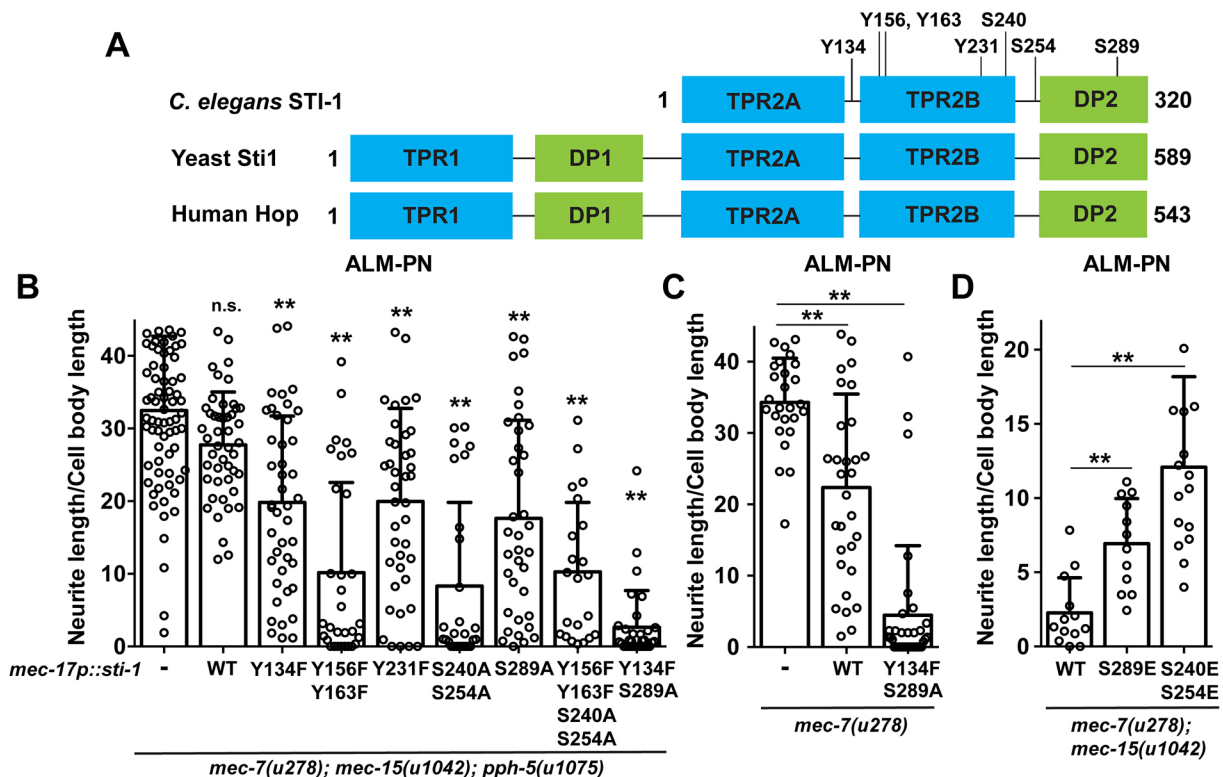

Fig. 3. Phosphorylation inhibits STI-1 activity. (A) Schematic representation of domain structure of *C. elegans* STI-1 and its yeast and human homologs. Potential phosphorylation sites for *C. elegans* STI-1 are shown. Numbers indicate amino acid positions. (B-D) The length of ALM-PN in *mec-7; mec-15; pph-5* triple mutants or *mec-7* single mutants or *mec-7; mec-15* double mutants in the absence of the *sti-1* transgene (−) or in the presence of the wild-type (WT) or the mutant STI-1 proteins expressed from the *mec-17* promoter. **P<0.01 between the control and the test group in ANOVA and Dunnett's tests. n.s., not significant. Data are mean±s.d. with individual data points indicated.

six and five phosphorylation sites, respectively, that are found mostly flanking the Hsp70-interacting TPR1 and TPR2B domains or in the linker region; those sites are not conserved and appear to be unique to the species (Röhl et al., 2015). Similarly, we predicted the presence of potential phosphorylation sites in *C. elegans* STI-1 flanking TPR2B and in the linker region, as well as the presence of the only phosphorylatable residue (S289) in the DP domain (Fig. 3A); those sites are mostly unique to *C. elegans* STI-1, except Y134 and Y163, which are conserved across yeast, human and *C. elegans*.

We reasoned that if PPH-5 regulated STI-1 activity through dephosphorylation, *pph-5(−)* mutants might have hyperphosphorylated STI-1 with low activity and the expression of non-phosphorylatable STI-1 in *pph-5* mutants might rescue STI-1 activity, and thus suppress the loss of *pph-5*. Indeed, TRN-specific expression of non-phosphorylatable STI-1 mutants, with one or several potential modification sites removed, suppressed the effect of *pph-5(−)* mutation to varying degrees in *mec-15(u1042); mec-7(u278)* animals (Fig. 3B). As a control, overexpression of wild-type STI-1 had little effect on ALM-PN growth in *pph-5; mec-15; mec-7* animals (Fig. 3B). Among the STI-1 mutants, S240A-S254A and Y134F-S289A most strongly suppressed the rescuing effects of *pph-5(−)* mutations on ALM-PN growth, suggesting that (1) those residues are key regulatory sites on STI-1; and (2) PPH-5 functions to activate STI-1. We should point out that PPH-5 is serine/threonine phosphatase and cannot dephosphorylate phospho-tyrosine. So the inhibitory effect of the tyrosine-to-phenylalanine changes on ALM-PN growth might result from the reduction of the overall phosphorylation level of STI-1 and is not specific to the loss of *pph-5*. PPH-5 probably acts through S240, S254 and S289 but not Y134.

Overexpression of STI-1(Y134F-S289A) mutants in *mec-7(u278)* animals also strongly suppressed the growth of ectopic ALM-PN (Fig. 3C), indicating that STI-1 dephosphorylation can significantly elevate its activity in destabilizing MTs and inhibiting neurite growth. Consistent with this notion, overexpression of phosphomimic and inactive STI-1 mutants (e.g. S240E-S254E) in *mec-15(u1042); mec-7(u278)* partially suppressed *mec-15(−)* mutation and restored ALM-PN in *mec-15; mec-7* animals, presumably by competing with endogenous STI-1 (Fig. 3D). The above data indicate that, similar to yeast and mammalian Sti1/Hop proteins, *C. elegans* STI-1 is regulated by inhibitory phosphorylation, and PPH-5 might activate STI-1 through dephosphorylation.

Mutations in chaperones rescue MT loss and synaptic defects of *mec-15* mutants

Consistent with the hypothesis that chaperones are detrimental to TRN development in *mec-15* mutants, we also observed suppressing effects of chaperone mutations on *mec-15(−)*-induced changes in MT organization. We previously showed that MT organization and stability determines neurite growth patterns in TRNs (Zheng et al., 2017). Using electron microscopy (EM), we found that the number of MTs in a cross-section of TRN neurite was dramatically reduced in *mec-15* mutants compared with the wild type in both ALM and PLM (Fig. 4A,B). For example, PLM-AN in *mec-15(u1042)* mutants had 4.9±2.9 (mean±s.d.) MTs on average in a cross-section, compared with 29.8±6.5 MTs in the wild type. In addition to the loss of MTs, *mec-15* mutants also had smaller MTs than the wild type. For example, whereas 98% (*n*=306) of the MTs in the wild type had the 15-protofilament (15-p) MTs, 71% (*n*=65) of the MTs in the PLM-AN of *mec-15(u1042)* adults had between 11 and 13 protofilaments, resulting in significantly smaller MT diameters (Fig. 4C,D). The loss of MTs and their smaller size indicate that MTs are highly unstable and disorganized in the absence of MEC-15.

The structural defects of MTs in *mec-15* mutants are rescued in *mec-15; sti-1* and *mec-15; pph-5* double mutants, which had restored MT numbers (16.2±4.3 and 17.6±9.2 MTs in the PLM-AN, respectively). The double mutants also have large-diameter 15-protofilament MTs, similar to those seen in the wild type (Fig. 4D). These data suggest that the loss of Hsp90 co-chaperones promotes MT formation and stability, which in turn rescues the TRN neurite growth defects in *mec-15* mutants.

Consistent with our previous finding that MT depolymerization in the TRNs causes a general reduction in protein levels (Bounoutas et al., 2011), *mec-15* mutants showed drastically decreased TagRFP expression from a *mec-17p::TagRFP* transgene in the TRNs, compared with the wild type (Fig. 4E). This reduction in protein level was completely rescued by mutations in *daf-41/p23*, *sti-1* and *pph-5* (Fig. 4E). Moreover, *mec-15* mutants also showed an almost complete loss of GFP::RAB-3 localization at the presynaptic site in PLM neurons and a partial loss in ALM neurons (Bounoutas et al., 2009b). This transport defect is probably caused by unstable MTs and is suppressed by the mutations in *sti-1* and *pph-5* (Fig. 4F).

TRNs are mechanosensory neurons that detect gentle touch to the body; this sensory function of TRNs depends on the 15-p MTs (Bounoutas et al., 2009a). Mutations in *mec-15* cause touch insensitivity (Chalfie and Au, 1989), probably due to the loss of 15-p MTs. This sensory defect was fully rescued in *sti-1; mec-15* and *pph-5; mec-15* double mutants, and partially rescued in *daf-41; mec-15* double mutants (Fig. 4G).

Thus, in addition to neurite development, the removal of the molecular chaperone pathway genes restored a variety of MT-related structures and functions affected by *mec-15* loss. Given the protective nature of the chaperones, this restoration is rather unexpected and suggests that Hsp70/Hsp90 machinery might contribute to the refolding and stabilization of a client protein or proteins that negatively affect MT stability and TRN development.

Hsp90 chaperones inhibit neurite growth by stabilizing DLK-1

As our *mec-15* suppressor screen (Table S1) yielded two *dlk-1 lf* alleles, *u1105* (V844I) and *u1138* (W394*), we examined the possibility that Hsp70/Hsp90 might regulate MT organization and neurite growth by acting on *dlk-1*, which encodes a MAP3 kinase that is homologous to human MAP3K12 and MAP3K13. Both *u1105* and *u1138* mutations restored the growth of both ALM-PN and PLM-PN in *mec-15(u1042); mec-7(u278)* mutants (Fig. 5A,B). The missense mutation (V844I) in *u1105* is adjacent to a C-terminal region (amino acids 850 to 881) of DLK-1 that interacts with its kinase domain (Yan and Jin, 2012); thus, catalytic function of DLK-1 might be impaired in *u1105* mutants. Another *dlk-1 lf* allele, *ju476* (a frameshift mutation), suppressed *mec-15(−)* even more strongly. The phenotype of *dlk-1(−)* is similar to the effects of *sti-1(−)* and *pph-5(−)* in *mec-15; mec-7* mutants. Independent of the *mec-7(u278)* background, *dlk-1 lf* alleles also suppressed the shortening of PLM-PN and the premature termination of PLM-AN in *mec-15(u1042)* mutants (Fig. 5C,D). Moreover, *dlk-1 lf* alleles showed maternal effects similar to *daf-41*, *sti-1* and *pph-5 lf* alleles (Fig. 5B). These data suggest that *dlk-1* might function in the same pathway as the chaperone and co-chaperone genes.

Expression of DLK-1a from the TRN-specific *mec-17* promoter rescued the loss of *dlk-1* by suppressing the growth of ALM-PN in *dlk-1; mec-15; mec-7* triple mutants, confirming that DLK-1 functions cell-autonomously (Fig. 5E). More importantly, overexpression of DLK-1a also suppressed the phenotype of *pph-5* and *sti-1* mutants, indicating that DLK-1 functions downstream of the chaperones (Fig. 5E). Through a yeast
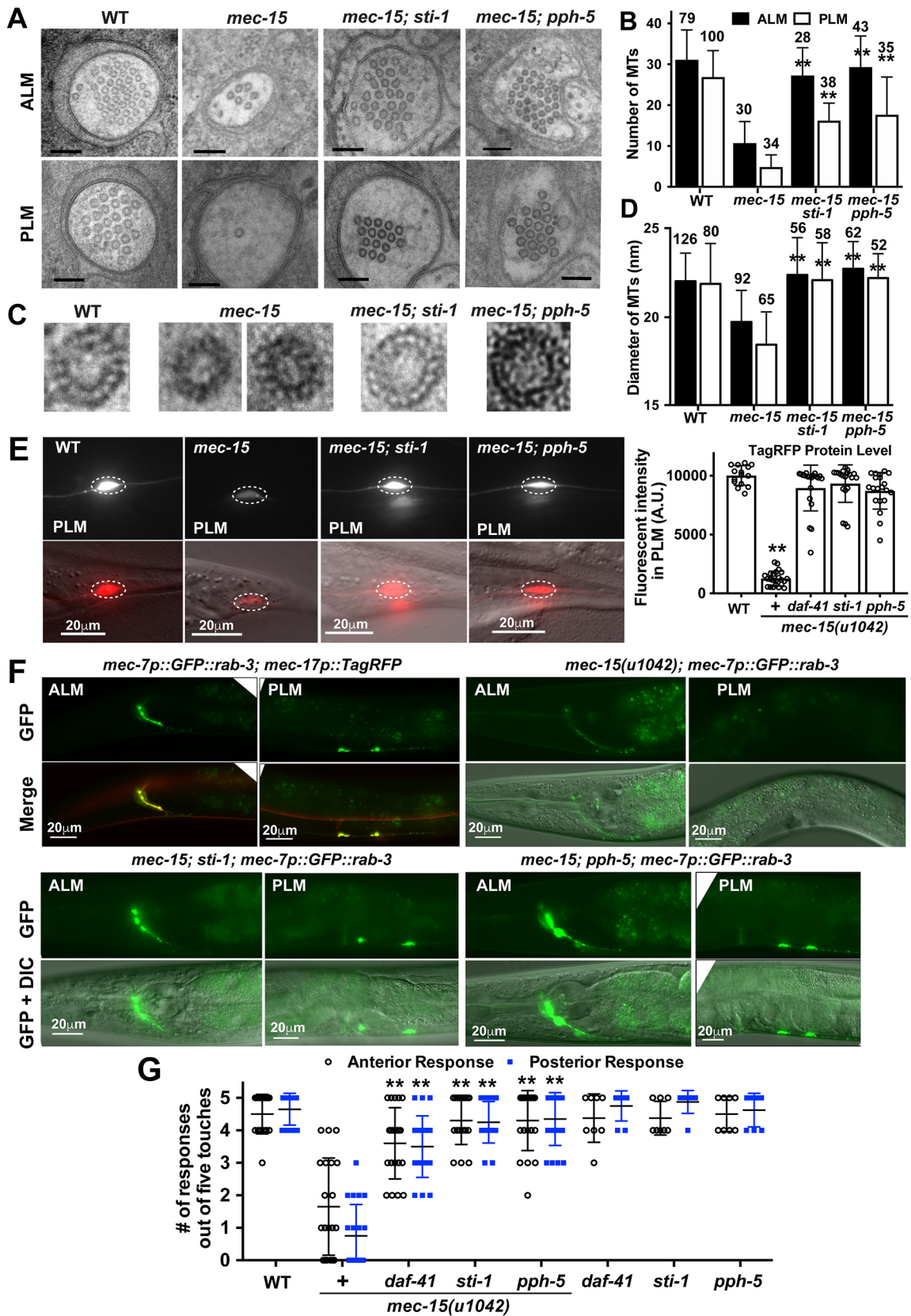
Fig. 4. See next page for legend.

two-hybrid assay, we detected a physical interaction between HSP90 and DLK-1a (Fig. 5F), which is the long and active isoform of DLK-1 (Yan and Jin, 2012). Moreover, the level of GFP::DLK-1a fusion protein was drastically reduced in *pph-5* and *sti-1* mutants, suggesting that the stability of DLK-1 relies on the Hsp90 chaperones (Fig. 5G).

Fig. 4. The loss of MTs and TRN developmental and functional defects in *mec-15* mutants was rescued by mutations in Hsp90 co-chaperones. (A) Representative EM micrographs of cross-sections of ALM-AN and PLM-AN in wild-type, *mec-15(u1042)*, *mec-15; pph-5(ok3498)* and *mec-15; sti-1(ok3354)* animals. Scale bars: 100 nm. (B) Average number of MTs in a cross-section of ALM-AN and PLM-AN in various strains. Numbers of sections analyzed for each strain are indicated above the bars. The sections are from at least ten animals. (C) Enlarged EM images of individual MTs with the protofilament visualized by tannic acid staining from the cross-sections of PLM-AN of the strains shown in A. (D) Average diameter of MTs in cross-sections from various strains. Number of MTs measured are indicated above the bars. In B and D, double asterisks indicate statistical significance (*P*<0.01) for the difference between *mec-15* mutants and the double mutants. (E) Fluorescent intensity of TagRFP in PLM expressed from the *uls115[mec-17p::TagRFP]* transgene in *mec-15(u1042)*, *mec-15; pph-5(ok3498)*, *mec-15; sti-1(ok3354)* and *mec-15; daf-41(ok3052)* mutants. Quantification is in arbitrary units (A.U.) for comparison. Representative images are shown with fluorescence only and fluorescence and DIC. (F) Localization of synaptic vesicles labeled by GFP::RAB-3 in TRNs of wild-type, *mec-15*, *mec-15; sti-1* and *mec-15; pph-5* animals. (G) The number of gentle touch responses from five gentle touch stimuli in the strains indicated at 20°C. Data are mean±s.d. **P<0.01 for the difference between *mec-15* mutants and the double mutants.

DLK-1 is known to induce MT dynamics and is essential for axonal regeneration in TRNs (Tang and Chisholm, 2016; Yan et al., 2009); DLK-1 signaling is also required for MT depolymerization-induced downregulation of protein levels in TRNs (Bounoutas et al., 2011). Indeed, *dlk-1 lf* mutations blocked the downregulation of TagRFP in *mec-15(−)* animals, whereas overexpression of DLK-1a in wild-type animals led to marked reduction of TagRFP expression (Fig. 5H). Consistent with a role in reducing MT stability, DLK-1a overexpression strongly suppressed the growth of ectopic ALM-PN in *mec-7(u278)* animals, and also shortened PLM-AN and PLM-PN in wild-type animals (Fig. 5C,E). The above data suggest that DLK-1 probably mediates the activity of Hsp90 chaperones and co-chaperones in destabilizing MTs during development. Coincidentally, a recent study found that Hsp90 is also a chaperone for DLK in mouse neurons and in *Drosophila*, and is required for axon injury signaling (Karney-Grobe et al., 2018). Thus, the regulation of DLK-1 by the Hsp90 chaperone appears to be evolutionarily conserved.

Importantly, DLK-1 is not the only downstream effector of the chaperones because, unlike the *sti-1* and *pph-5 lf* mutations, the *dlk-1 lf* mutations did not rescue the touch insensitivity, PLM-AN branching defects or the GFP::RAB-3 localization defect in *mec-15* mutants (Fig. S6). Even with neurite growth, the loss of *dlk-1* did not fully rescue the outgrowth defect of PLM-PN and PLM-AN in *mec-15* mutants (Fig. 5C,D). Thus, we expect that other Hsp90 client proteins also function during TRN development.

MEC-15 downregulates DLK-1 levels in TRNs
As MEC-15 is a F-box protein that probably functions in an SCF complex to target substrate protein for ubiquitylation and degradation, we next investigated whether MEC-15 regulates DLK-1 protein levels. We found that the expression of GFP::DLK-1 fusion proteins was elevated in *mec-15* mutants (Fig. 5G), whereas the levels of STI-1::GFP and PPH-5::GFP fusion proteins were not changed in *mec-15* mutants (Fig. S7A). Importantly, the level of GFP::DLK-1 was also increased by blocking ubiquitylation through TRN-specific silencing of *uba-1* (Fig. 5G). Thus, MEC-15 probably targets DLK-1 but not the Hsp90 co-chaperones for degradation.

We could not detect any physical interaction of MEC-15 with DLK-1a in yeast two-hybrid assays, which suggests that the interaction may be transient or dependent on a particular post-translational modification of DLK-1. We also did not detect any interaction of MEC-15 with STI-1, PPH-5, DAF-41, HSP-90 or

HSP-110. In an attempt to detect MEC-15 binding to DLK-1 in the TRNs, we made constructs that expressed HA-tagged MEC-15 and FLAG-tagged DLK-1 from the TRN-specific *mec-18* and *mec-17* promoters, respectively. When we injected the two expression constructs into worms separately, both MEC-15 and DLK-1 could be detected by probing the tags using a western blot; but when injected together, only MEC-15::HA was detected, and FLAG::DLK-1 was undetectable (Fig. S7B). Although this rendered a co-immunoprecipitation assay impossible, these results suggested that MEC-15 suppressed the expression of DLK-1 protein.

RPM-1, a RING-finger E3 ubiquitin ligase, also downregulates the abundance of DLK-1 at the protein level and modulates the p38 MAP Kinase pathway (Nakata et al., 2005). The phenotype of *rpm-1* mutants, however, is the direct opposite of *mec-15* mutants. Instead of the shortened TRN neurites of *mec-15* mutants, *rpm-1(ok364)* knockout mutants had overextended ALM-AN and PLM-AN (Fig. S7C; Schaefer et al., 2000). Moreover, the loss of *rpm-1* did not suppress the ectopic ALM-PN in *mec-7(u278)* mutants, and the *rpm-1 mec-7* double mutants showed long ALM-PN and the overextension of ALM-AN and PLM-AN (Fig. S7D-F). Thus, RPM-1 appears to negatively regulate neurite growth, whereas MEC-15 promotes growth. Downstream of both proteins, DLK-1 might exert dual functions in inducing MT dynamics and promoting neurite extension, depending on the cellular contexts.

mec-15 is epistatic to *rpm-1* as *mec-15; rpm-1* double mutants showed mostly the *mec-15(−)* phenotype, having shortened PLM-ANs and PLM-PNs. The *mec-15; rpm-1; mec-7* triple mutants showed the phenotype of *mec-15; mec-7* double mutants in the suppression of ALM-PN (Fig. S7E,F). This epistasis suggests that either MEC-15-mediated regulation of DLK-1 plays a more dominant role in TRNs than RPM-1-mediated regulation, or that MEC-15-regulated DLK-1-independent pathways act downstream of RPM-1.

MEC-15 regulates the function of GABAergic motor neurons by antagonizing Hsp90 chaperone activities
Finally, the genetic interaction between *mec-15* and the Hsp90 chaperones occurs not only in the TRNs but also in other neurons. In the ventral cord motor neurons, MEC-15 regulates the trafficking of synaptic vesicle protein SNB-1 and promotes GABAergic synaptic transmission (Sun et al., 2013). We found that *mec-15* mutants had fewer synaptic puncta labeled by SNB-1::GFP in GABAergic neurons than wild-type animals (Fig. 6A-C). This deficit in synaptic density was rescued by mutations in *sti-1* or *pph-5*, although the average fluorescent intensity of each punctum was similar between the mutants and the wild-type animals (Fig. 6A-C).

Behaviorally, reduced GABA release in *mec-15* mutants led to lower inhibitory postsynaptic currents in the body wall muscles and increased sensitivity to the acetylcholine esterase inhibitor aldicarb, which causes paralysis through the accumulation of acetylcholine and persistent muscle contraction (Sun et al., 2013). This increased sensitivity to aldicarb in *mec-15* mutants was completely suppressed in *mec-15; sti-1* and *mec-15; pph-5* mutants (Fig. 6D). Therefore, MEC-15 and Hsp90 chaperones also appear to counter each other to regulate GABAergic synaptic function. Moreover, similar to the thermosensitive PLM-AN growth defects in *mec-15* mutants, we found that *mec-15(−)* animals grown at 25°C are much more sensitive to aldicarb than animals raised at 20°C; loss of *sti-1* or *pph-5* also rescued this temperature-dependent defect (Fig. 6D). These results suggest that MEC-15 target proteins in both TRNs and GABAergic motor neurons are more stable or have higher levels at higher temperatures, probably because of the increased activity of Hsp90 chaperones at higher temperatures.
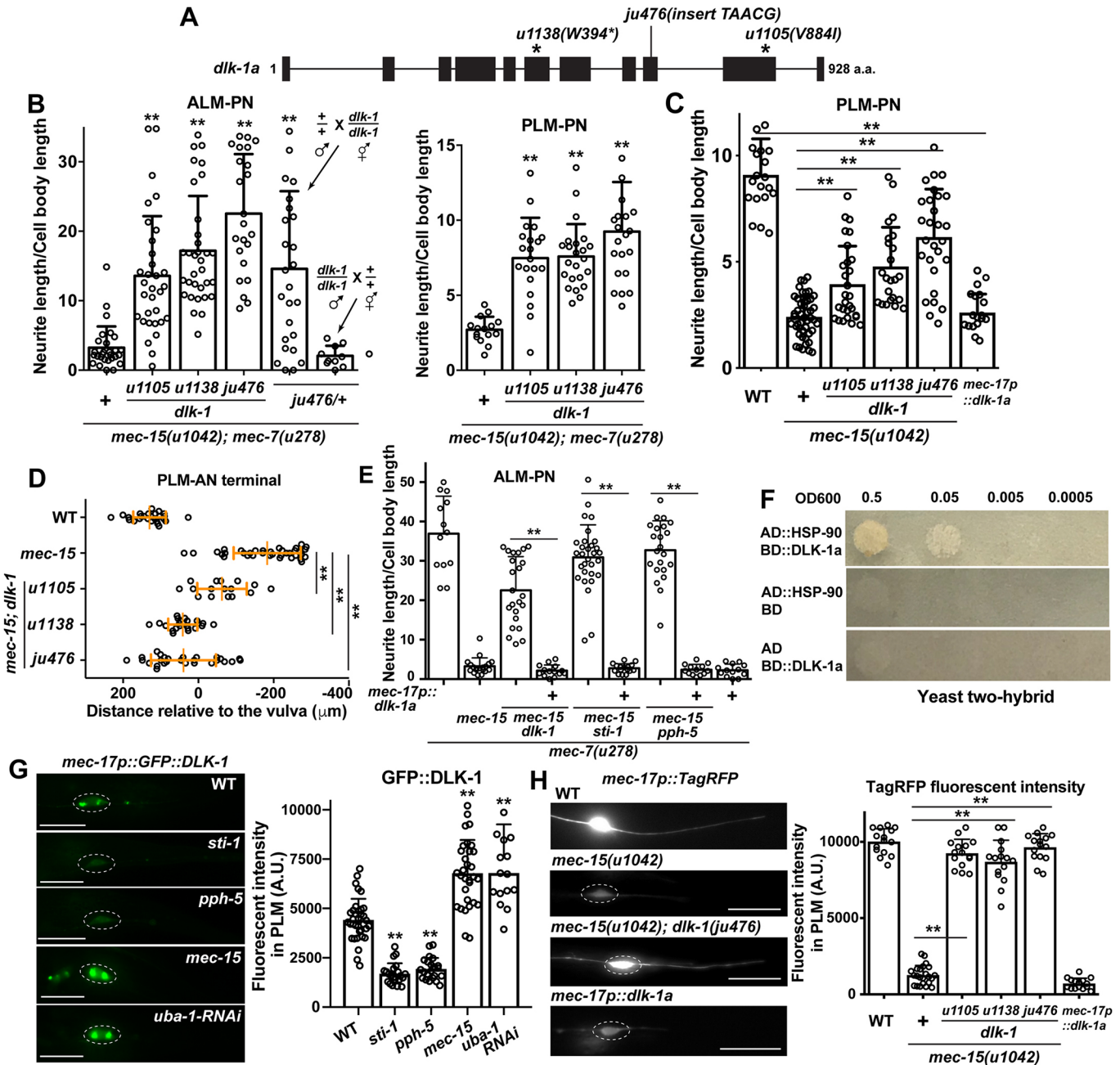
DEVELOPMENT

8

Fig. 5. DLK-1 acts downstream of the chaperones to destabilize MTs and inhibit neurite growth. (A) Gene structure of the long isoform (a) of *dlk-1* and the positions of three *lf* mutations. (B) Effects of *dlk-1* mutations on the normalized neurite length of ALM-PN and PLM-PN in *mec-15(u1042); mec-7(u278)* animals. The ALM-PN length in *ju476/+* animals was examined in male cross progeny. **P<0.01 between the test group and *mec-15; mec-7* double mutants. (C) The length of PLM-PN in *dlk-1; mec-15* mutants and wild-type animals expressing the *mec-17p::dlk-1a* transgene. (D) The distance between the PLM-AN terminal and the vulva in the *dlk-1; mec-15* mutants grown at 25°C. (E) The length of ALM-PN in *mec-7(u278)* animals with indicated mutant genotype. Some animals expressed a *mec-17p::dlk-1a* transgene. The *dlk-1(ju476)*, *sti-1(ok3354)* and *pph-5(ok3498)* alleles were used. (F) Yeast two-hybrid assays for the interaction between AD::HSP-90 and BD::DLK-1a. AD means the Gal4 activation domain and BD means the Gal4 DNA-binding domain. (G) Fluorescent intensity of GFP::DLK-1 expressed from the TRN-specific *mec-17* promoter in wild type, *sti-1(ok3354)*, *pph-5(ok3498)* and *mec-15(u1042)* mutants, and animals carrying the *mec-17p::uba-1RNAi* transgenes. Dashed circles enclose PLM cell bodies; scale bar: 20 µm. Double asterisks indicate significant difference from the wild type (WT). (H) Fluorescent intensity of TagRFP expressed from *mec-17* promoter in *dlk-1; mec-15* double mutants and in wild-type animals expressing the *mec-17p::dlk-1a* transgene. A.U., arbitrary units. Data are mean±s.d. (**P<0.01).

DISCUSSION

Ubiquitylation and protein degradation promote stable MTs and neurite growth

The UPS affects many processes of neuronal development, including neurogenesis, cell fate specification, neuronal migration, polarization and axonal and dendrite morphogenesis (Tuoc and Stoykova, 2010; Yamada et al., 2013). With respect to neurite morphogenesis, previous studies suggested that E3 ubiquitin ligase can both positively and negatively regulate neurite growth. For example, during axodendritic polarization in hippocampal neurons, the HECT-domain E3 ubiquitin ligase Smurf1 promotes the growth of axons by degrading RhoA (inhibitor of axon growth), whereas
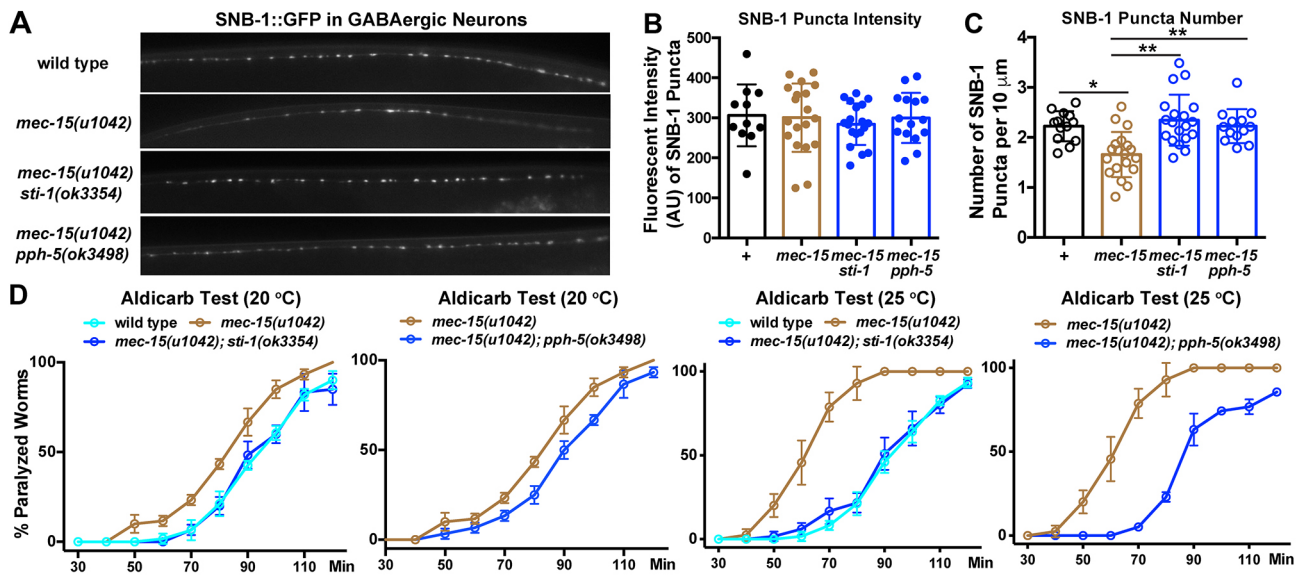
Fig. 6. MEC-15 regulates synaptic functions of GABAergic motor neurons by antagonizing the activity of Hsp90 chaperones. (A) Synaptic puncta in the ventral neurite of GABAergic motor neurons labeled by *juIs1[unc-25p::snb-1::GFP]* in the wild-type animal, *mec-15*, *mec-15; sti-1* and *mec-15; pph-5* mutants. (B) Average fluorescent intensity (A.U., arbitrary units) of the SNB-1::GFP puncta in the indicated strains. (C) Average number of SNB-1::GFP puncta in 10 μm of the ventral neurite of GABAergic motor neurons in the indicated strains. (D) Percentage of adult animals paralyzed at the indicated time point after being exposed to 1 mM aldicarb. Animals were raised from embryos to young adults at either 20°C or 25°C before the test. Twenty animals and three replicates were used in each experiment. The experiment was repeated three times. Data are mean±s.d. The same *mec-15* data were plotted twice in the two graphs for comparison with the double mutants (*$P<0.05$ and **$P<0.01$).

Smurf2 inhibits the growth of neurites fated to be dendrites by degrading Ras GTPase Rap1B (inducer of neurite growth; Cheng et al., 2011; Schwamborn et al., 2007).

Our studies identified the F-box and WD40 domain protein MEC-15 (ortholog of human FBXW9) as a positive regulator of neurite growth. As in the above examples, MEC-15 presumably functions in an SCF-containing complex, which is an E3 ubiquitin ligase, to degrade protein(s) that can inhibit neurite outgrowth. One potential substrate of MEC-15 is the MAP3 kinase DLK-1, which is known to induce MT dynamics (Tang and Chisholm, 2016) and can suppress neurite growth when overexpressed (this study). As the loss of *dlk-1* did not fully rescue the developmental defects of *mec-15(−)* mutants, MEC-15 probably has multiple substrates.

In the PLM neurons, the anterior neurite is considered an axon because its MTs has uniform 'plus-end out' polarity, whereas the posterior neurite is more like a dendrite given that its MTs have mixed polarity (Hsu et al., 2014). MEC-15 is required for the extension of both PLM-AN and PLM-PN, which suggests that MEC-15 is a general regulator of neurite growth instead of an axon- or dendrite-specific regulator, like the E3 ligase Cdh1-APC and Cdc20-APC (Konishi et al., 2004). This function of MEC-15 might be attributed to its activity in promoting the formation of stable MTs as mutations in *mec-15* led to a significant loss of MTs and the reduction of MT diameters. Thus, our studies link the SCF complex and UPS to the general stability of MT cytoskeletons.

Dual yet contradictory functions of DLK-1
Another conserved RING-domain E3 ubiquitin ligase, RPM-1, also regulates neurite extension in TRNs by interacting with the SCF complex, including SKR-1/Skp, CUL-1/Cullin and the F-box protein FSN-1/FBXO45 (Nakata et al., 2005). However, MEC-15 and RPM-1 have opposing functions. MEC-15 promotes neurite growth, whereas RPM-1 inhibits neurite growth. More surprisingly, both RPM-1 and MEC-15 appear to target DLK-1 for degradation.

As mutations in *dlk-1* partially suppress both the overextension phenotype in *rpm-1(−)* mutants (Nakata et al., 2005) and the underextension in *mec-15(−)* mutants (this study), DLK-1 might exhibit dual yet opposite functions in regulating neurite growth.

Elevated DLK-1 levels promote axon growth in *rpm-1(−)* mutants but inhibit neurite growth in *mec-15(−)* mutants; these two opposing functions seem to be balanced under normal conditions as *dlk-1(−)* mutants did not show any TRN morphological defects. Perhaps the spatial and temporal expression of DLK-1 determines which of the two opposing functions is engaged. For example, DLK-1 may play inhibitory roles for general neurite extension during the growth phase by reducing MT stability globally in the entire cell and then prevent axon termination at specific sites at a later stage of development. Because *mec-15(−) rpm-1(−)* double mutants exhibited the underextension phenotype, the overall effects of accumulating DLK-1 appear to inhibit neurite growth. Interestingly, DLK-1 also initiates apparently contradictory responses under stress conditions during development and after axonal injury (Tedeschi and Bradke, 2013). For example, after optical nerve injury in mice, DLK triggers the expression of both pro-apoptotic and regenerative genes, although cell death is the dominant response (Watkins et al., 2013). Future studies are needed to understand how the multifaceted functions of DLK-1 are controlled spatially and temporally to initiate specific signaling. Our work also suggests that different components of the UPS could generate distinct cellular responses by targeting the same protein.

Inhibitory role of Hsp70/Hsp90 chaperones and co-chaperones in neuronal development
Besides the protective effects of Hsps in cells under stressed conditions, growing evidence suggests that these chaperones also play regulatory roles in normal neurodevelopment (Miller and Fort, 2018). The ATP-dependent Hsp70 and Hsp90 family chaperones

are expressed in the nervous system during mouse embryonic and postnatal development, which suggests that they may function in both neurogenesis and late-stage neurodevelopment (Loones et al., 2000). In fact, the deletion of the transcription factor HSF1, which activates the transcription of many Hsp genes, led to impaired olfactory neurogenesis, and hippocampal spinogenesis and neurogenesis in mice (Uchida et al., 2011), supporting a crucial role for Hsps in proper neurodevelopment.

At the subcellular level, Hsc70 (Hsp70 family chaperone) and Hsp90 are localized to the apical dendrites of Purkinje cells and cerebellar neurons from the postnatal period into adulthood (D'Souza and Brown, 1998); in the differentiating hippocampal neurons, Hsp90 was associated with the cytoskeleton in branch points and terminal ends (Quintá and Galigniana, 2012). These results suggest that Hsps may regulate neuronal polarization and neurite morphogenesis by modulating cytoskeleton dynamics. Indeed, pharmacological inhibition of Hsp90 disturbed the polarization and axonal extension of cultured hippocampal neurons by inhibiting the PI3K/Akt/GSK3 signaling pathway (Benitez et al., 2014), which is known to regulate neuronal morphogenesis (Kim et al., 2011). The fact that Akt and GSK3 are Hsp90 client proteins (Banz et al., 2009; Sato et al., 2000) indicates that Hsp90 could regulate cell differentiation by maintaining the stability of its client proteins. Thus, given that Hsp90 interacts with hundreds of client proteins, the specific function of Hsp90 in differentiation would depend on the function of its client protein(s) in particular cellular contexts.

Our studies identified one such context, in which Hsp70/Hsp90 chaperones play an unexpected inhibitory role in regulating MT stability and neurite growth. In mec-15(−) mutants, Hsp70/Hsp90 chaperone and co-chaperones contribute to destabilizing MTs, inhibiting neurite growth, suppressing synaptic development and disrupting sensory functions. Components of this molecular chaperone machinery include HSP-110/Hsp70, HSP-90/Hsp90, co-chaperone STI-1/STI1/Hop (which links Hsp70 and Hsp90), PPH-5/PP5 (which interacts with and activates Hsp90 and other co-chaperones through dephosphorylation), DAF-41/p23/PTGES3 (which binds to Hsp90 in its ATP-bound conformation and stabilizes the Hsp90-substrate complexes) and CDC-37/Cdc37 (which interacts with Hsp90 and promotes the maturation of kinase substrate) (Fig. 7). Removing any of these components in mec-15(−) mutants rescued the TRN developmental defects and restored normal differentiation. The fact that our experiments identified

almost every component in an Hsp90 ATPase cycle (or protein folding cycle) suggests that a complete Hsp90 pathway is involved in negatively regulating TRN differentiation.

At least part of this negative regulation is mediated by the stabilization of DLK-1, which is a conserved Hsp90 client protein in C. elegans (this study), Drosophila and mice (Karney-Grobe et al., 2018). Because the loss of Hsp90 co-chaperones fully rescued all developmental defects in mec-15(−) mutants, whereas mutations in dlk-1 only partially suppressed the neurite growth defects, other client proteins stabilized by Hsp90 chaperones might also participate in the inhibition of TRN differentiation. Future studies will focus on identifying such clients.

The opposing effects of UPS and chaperones in neuronal differentiation
Mutations in the chaperones and co-chaperones by themselves did not produce any defects in TRN differentiation, suggesting that the inhibitory function of Hsp70/Hsp90 chaperones and co-chaperones does not seem to affect normal development. This lack of effect might be due to Hsp90 clients, such as DLK-1, being normally maintained at a low level by the UPS involving MEC-15, making the effects of chaperone loss difficult to detect. In mec-15(−) mutants, DLK-1 and perhaps other Hsp90 client proteins are stabilized by the Hsp70/Hsp90 chaperone machinery, accumulate in the TRNs and exert their functions. In such scenarios, the activity of chaperones in controlling differentiation becomes crucial. Thus, by targeting the Hsp90 clients for degradation, UPS curbs the activity of the chaperones in inhibiting cellular differentiation.

These opposing effects of UPS and the chaperones are quite unexpected as most previous studies indicate that they work synergistically to degrade misfolded proteins. This protein quality control safeguards axon guidance in developing neurons (Wang et al., 2013) and prevents protein aggregation that leads to neurodegeneration (Ciechanover and Kwon, 2017). Our studies, however, provide novel insights into the interaction between the UPS and the chaperones by suggesting that chaperones also promote the expression and stabilization of proteins that are normally degraded by UPS for fast turnover and low background abundance. This tug-of-war keeps the common substrate of the UPS and the chaperones at the optimal level, which is crucial for a range of neurodevelopmental processes, including MT formation, neurite growth, synaptic development and neuronal functions, not only in the TRNs but also in the GABAergic motor neurons. Therefore, we
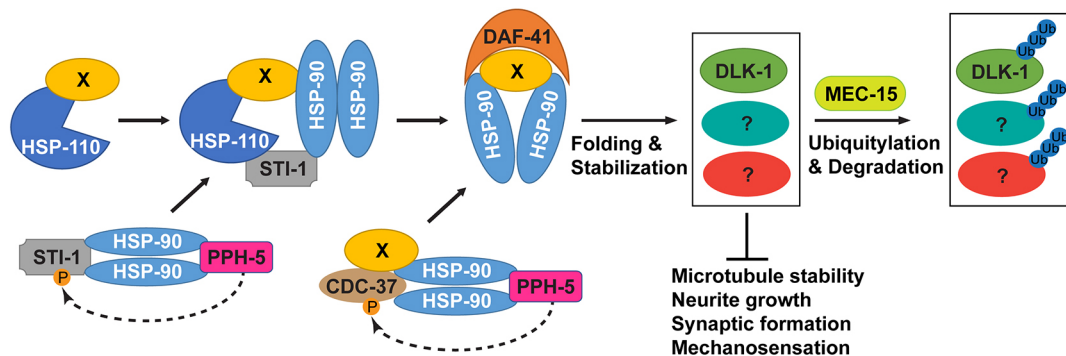

Fig. 7. A model for the antagonism between the activities of Hsp70/Hsp90 chaperone machinery and MEC-15 in the regulation of TRN differentiation and functions. HSP-90 receives client protein X from either HSP-110 (a Hsp70 family protein) via a STI-1-mediated physical link or CDC-37 via its binding to kinase clients. Both STI-1 and CDC-37 are activated by PPH-5 through dephosphorylation (dashed line). Those Hsp90 client proteins, including DLK-1 and other unidentified proteins (?), are not only stabilized by the chaperones but also subjected to MEC-15-mediated ubiquitylation and degradation. The antagonism between the chaperones and MEC-15 tightly controls the levels of those Hsp90 client proteins, which appear to negatively regulate MT stability, neurite growth and synaptic development.

suspect that the balance between the UPS and chaperone activities might be generally important for robust neuronal differentiation.

MATERIALS AND METHODS
Strains and forward genetic screens
C. elegans wild-type (N2) and mutant strains were maintained at 20°C as described previously (Brenner, 1974). Alleles used in this study are described in the Results. Most strains were provided by the *Caenorhabditis* Genetics Center, which is funded by the National Institutes of Health Office of Research Infrastructure Programs (P40 OD010440), or provided by the National BioResource Project of Japan.

For the *mec-7(neo)* suppressor screen, we used TU4879 [*mec-7(u278) X; uIs115(mec-17p::TagRFP) IV*] as the starter strain, which showed the growth of a long ALM-PN, and ethyl methanesulfonate (EMS) as the mutagen (Brenner, 1974). We isolated 30 mutants that showed very short or no ALM-PN and outcrossed the mutants against TU4879, and identified the phenotype-causing mutations through a combination of whole-genome resequencing, candidate gene sequencing and complementation tests. *mec-15(u1042)* was isolated from this screen; details about other suppressors will be reported elsewhere.

For the *mec-15(−)* suppressor screen, we used TU5183 [*mec-15(u1042); mec-7(u278); uIs115*] as the starter strain, which had a short or no ALM-PN, and EMS as the mutagen. Through a screen of 29,153 haploid genomes, we isolated 12 mutants that had a prominent ALM-PN with at least five cell body lengths and identified the phenotype-causing mutations in eight of the mutants through whole-genome resequencing (Table S1). Deletion alleles *sti-1(ok3354)* and *pph-5(ok3498)*, and frameshift-causing allele *dlk-1(ju476)*, were used as the reference alleles.

Candidate RNAi screen
To test Skp and Cullin homologs for the suppression of *mec-7(u278)*, we constructed TU6023 [*eri-1(mg366ts) uIs115 IV; mec-7(u278) lin-15b(n744) X*] for enhanced RNAi effects and performed feeding RNAi using bacteria colonies from the Ahringer library (Fraser et al., 2000). Briefly, we seeded bacteria expressing dsRNA on nematode growth plates (NGM), agar plates containing 6 mM isopropyl β-d-1-thiogalactopyranoside and 100 µg/ml ampicillin. One day later, eggs from TU6023 animals were placed onto these plates, hatched and grown to adults at 20°C. The F1 progeny of these worms were examined for the growth of ALM-PN at the day 1 adult stage. Genes that, when knocked down, shortened the ALM-PN length to below five cell bodies were regarded as positive.

To test candidate genes for the suppression of the *mec-15(−)* mutation, we constructed TU6092 [*mec-15(u75); eri-1(mg366) uIs115; mec-7(u278) lin-15B(n744)*] and performed feeding RNAi for the genes indicated in Table S2. Genes that, when knocked down, restored the ALM-PN length to above five cell bodies were regarded as positive; positives from the screen were confirmed using deletion alleles, including *hsp-90(ok1333)*, *hsp-110(gk533)* and *daf-41(ok3052)*.

Constructs and transgenes
For *mec-15* reporter and expression constructs, a *mec-15::GFP* translational reporter (TU2278) was made by cloning a 3.2 kb promoter upstream of the translational start and the entire *mec-15*-coding sequence into the pPD95.75 backbone, and was used to generate an integrated transgene *unkIs1[mec-15::GFP]*. *mec-18p::mec-15* (TU891) was generated previously by inserting a 0.5 kb *mec-18* promoter and the *mec-15*-coding sequence, with a 1.6 kb 3′UTR, into the pBlueScript II backbone (Bounoutas et al., 2009b). *mec-18p::mec-15(Δ9-50)* (TU2100), *mec-18p::mec-15(Δ9-84)* (TU2101) and *mec-18p::mec-15::HA* (CGZ84) were generated via site-directed mutagenesis using TU891 as a template.

For *pph-5* and *sti-1* reporter and expression constructs, the *pph-5* transcriptional reporter transgene *avIs90[pph-5p::mCherry::H2B::pph-5 3′ UTR; unc-119(+)]* was generated by Richie et al. (2011). For the *pph-5* translational reporter, we amplified a 2.3 kb promoter, the cDNA of *pph-5* (isoform a) and a 481 bp *pph-5* 3′UTR, and assembled the PCR products with amplified pUC57 backbone via HiFi assembly (New England Biolabs)

to generate the vector *pph-5p::pph-5(cDNA)::pph-5 3′ UTR* (TU2257). The GFP-coding sequence was then subcloned from pPD95.75 and inserted before the stop codon of *pph-5* to generate *pph-5p::pph-5(cDNA)::GFP:: pph-5 3′UTR* (TU2267) via HiFi assembly. The *sti-1p::GFP::unc-54 3′ UTR* (TU2202) transcriptional reporter was generated using the Gateway system (Life Technologies) by cloning a 1045 bp promoter into pDONR-P4-P1r and then performing LR reactions with pENTR-GFP, pENTR-unc-54-3′ UTR and destination vector pDEST-R4-R3. We then generated the *sti-1p::sti-1::sti-1 3′ UTR* vector (TU2264) by amplifying the backbone plus the *sti-1* promoter from TU2202 and the *sti-1* genomic coding sequence plus a 607 bp 3′ UTR from genomic DNA, and assembled them via HiFi assembly. GFP-coding sequence was then inserted before the *sti-1* stop codon to generate *sti-1p::sti-1::GFP::sti-1 3′ UTR* (TU2280).

For TRN-specific expression or RNAi constructs, *mec-17p::pph-5(cDNA)::pph-5 3′ UTR* (TU#2266) was generated by swapping the *pph-5* promoter in TU2257 with a 2.9 kb *mec-17* promoter. *mec-17p::sti-1::unc-54 3′UTR* (TU2166), *mec-17p::daf-41::FLAG::unc-54 3′UTR* (CGZ92) and *mec-17p::FLAG::dlk-1a::unc-54 3′UTR* (CGZ78) were generated by cloning the *mec-17* promoter and *sti-1*, *daf-41* and *dlk-1a* genomic coding sequences into the Gateway vectors and then performing the LR reactions with pENTR-unc-54-3′ UTR and pDEST-R4-R3. GFP was inserted into CGZ78 after the start codon of *dlk-1* to make *mec-17p::GFP::dlk-1a::unc-54 3′ UTR* (CGZ71). Various *mec-17p::sti-1* mutant constructs were generated by site-directed mutagenesis using TU2166 as a template. For TRN-specific RNAi of *uba-1*, *hsf-1* and *cdc-37*, we amplified the sense and antisense sequences of their genomic coding region (without start and stop codons), and inserted them downstream of a *mec-17* promoter in pDEST-R4-R3 backbones; the resulting constructs *mec-17p::uba-1-sense* (TU2286), *mec-17p::uba-1-antisense* (TU2287), *mec-17p::hsf-1-sense* (CGZ97), *mec-17p::hsf-1-antisense* (CGZ98), *mec-17p::cdc-37-sense* (CGZ82) and *mec-17p::cdc-37-antisense* (CGZ83) were injected in pairs into *mec-7(u278)* or *mec-15; mec-7* animals for RNAi. As negative controls for RNAi, we injected *mec-17p::gfp-sense* (CGZ167) and *mec-17p::gfp-antisense* (CGZ168) into corresponding animals to express dsRNA against GFP.

To generate transgenic animals, we injected DNA constructs (5 ng/µl for each expression vector) into the animals to establish stable lines carrying an extrachromosomal array; at least three independent lines were tested. In some cases, we integrated the arrays into the genome through standard γ-irradiation (Mello and Fire, 1995) to generate integrated transgenes, including *unkIs1[mec-15::GFP]* and *unkIs2[mec-17p::GFP::dlk-1]*. Those integrated lines were outcrossed at least five times before being examined.

Transgenes *uIs31[mec-17p::GFP] III*, *uIs115[mec-17p::RFP] IV* and *uIs134[mec-17p::RFP] V* were used to visualize TRN morphology (Zheng et al., 2015). *jsIs821[mec-7p::GFP::RAB-3]* was used to assess synaptic vesicle localization (Bounoutas et al., 2009b). *sEx10796[daf-41p::GFP]* was used to examine the *daf-41* expression pattern. *juIs1[unc-25p::SNB-1-GFP]* was used to examine synaptic puncta in the GABAergic motor neurons.

Electron microscopy
We fixed TU4065 [*uIs115(mec-17p::TagRFP)*], TU5598 [*mec-15(u1042); uIs115*], TU5579 [*pph-5(ok3498); mec-15(u1042); uIs115*] and TU5580 [*sti-1(ok3354); mec-15(u1042); uIs115*] adults grown at 20°C using either a chemical immersion (Hall, 1995) or a modified high-pressure freezing/freeze substitution (HPF/FS) protocol (Zheng et al., 2017). Chemical immersion was performed using 1% glutaraldehyde+1% tannic acid in 0.1 M phosphate buffer (pH 7.0); and high pressure freezing/freeze substitution was carried out with a first fixation in 0.5% glutaraldehyde+0.2% tannic acid at −90°C for 90 h and then at −60°C for 4 h, followed by a second fixation in 2% osmium tetroxide+0.2% uranyl acetate at −60°C for 16 h and then at −30°C for 16 h.

Transverse sections (80 nm) were collected at multiple positions along both the ALM anterior neurite and the PLM anterior neurites, and post-stained with uranium acetate and lead citrate. A JEOL JEM-1400Plus TEM with a Galan Orius SC1000B bottom-mount digital camera or a Philips CM10 electron microscope with an attached Morada digital camera (Olympus) was used to acquire the images. For each strain, we examined

DEVELOPMENT

sections from at least ten animals. For each animal, we collected sections from at least five different positions along the neurite and counted the number of MTs in a cross-section, measured the MT diameter and counted the number of protofilaments in individual MTs, of which clear substructure were observed. Data from ALML and ALMR were combined and PLML and PLMR combined. The number of data points for each measurement is indicated in Fig. 4B,D.

Yeast two-hybrid assay and western blot
Yeast media and plates were prepared according to recipes from Clontech and yeasts were grown at 30°C. The yeast strain PJ69-4a used for the two-hybrid assays contains GAL1-HIS3, GAL2-ADE2 and GAL7-lacZ reporters (Zheng et al., 2018). Vectors pGAD424 and pGBT9 (Clontech) were used to express proteins fused to the yeast-activating domain (AD) and yeast-DNA-binding domain (BD), respectively. cDNA fragments of *mec-15*, *skr-1*, *hsp-90* and *dlk-1a* were cloned into the two-hybrid vectors using HiFi Assembly (NEB).

Combinations of the AD or BD vectors were co-transformed into yeast using the Frozen-EZ II Kit (Zymo Research) and using empty vectors as negative controls. Growth assays were performed by growing individual colonies overnight in selective media lacking tryptophan and leucine, and then diluting the cultures to OD600=0.5; a series of further 1:10 dilutions were made and 10 µl of the diluted cultures were spotted onto plates lacking histidine to test the expression of the HIS3 reporter. Plates were imaged after 2 days of growth.

For western blot, transgenic animals were collected and lysed with radioimmunoprecipitation buffer [25 mM Tris-HCl (pH 7.5); 100 mM NaCl, 1 mM EDTA, 0.5% NP-40 and freshly added protease inhibitors] and sonicated for 15 cycles of 1 s on and 15 s off. The protein lysate was then separated by SDS-PAGE and blotted with anti-HA (1:500; TransGen Biotech, HT301-02) and anti-FLAG (1:1000; Sigma-Aldrich, F1804) primary antibodies and HRP-conjugated secondary antibodies (1:20,000; Sigma-Aldrich, A9044).

Fluorescent imaging, aldicarb assay, phenotype scoring and statistical analysis
Fluorescent imaging was performed either on a Zeiss Axio Observer Z1 inverted microscope equipped with a CoolSNAP HQ2-FW camera (Photometrics) or a Leica DMi8 inverted microscope equipped with a Leica DFC7000 GT monochrome camera. Measurements were made using either the Zeiss AxioVision (SE64 Rel. 4.9.1) or the Leica Application Suite X (3.7.0.20979) software.

We measured the length of TRN neurites in at least 20 larvae or young adults grown at 20°C, except where otherwise stated. Normalized neurite length was calculated by dividing the neurite length by the diameter of the cell body along the anterior-posterior axis. Defects in PLM-AN growth were assessed by measuring the distance from the PLM-AN terminals to the center of the vulva. Positive numbers mean PLM-AN terminals were more anterior than the vulva; negative numbers mean the PLM-AN did not reach the vulva; at least 30 cells were examined for each strain. All bar graph data are mean±s.d.

Fluorescence intensity of the TagRFP expressed from the *uIs115[mec-17p::TagRFP]* transgene or the GFP expression from the *unkIs2[mec-17p::GFP::dlk-1]* transgene in the PLM cell body, was used to measure TRN protein levels; intensity was measured by first acquiring images using the identical exposure time and laser power, and then manually subtracting the background from the fluorescent signal using ImageJ. At least 30 cells were imaged and analyzed for each strain.

For the aldicarb (an acetylcholinesterase inhibitor) sensitivity assay, 20 1-day-old adult animals were transferred onto NGM plates containing 1 mM aldicarb (Sigma-Aldrich) without food. The number of animals that were paralyzed was recorded every 10 min, starting at 30 min after the transfer. Genotypes were blind to the experimenter, and the assay was repeated three times.

For statistical analysis, analysis of variance and the post-hoc Dunnett's test (comparison of each of many treatments with a single control) or Tukey–Kramer test (studentized range test for all pairwise comparison) were performed using GraphPad Prism (version 8.00 for Mac, GraphPad

Software; www.graphpad.com) to identify significant difference among samples. Student's *t*-test was used to find significant difference between two samples in paired comparisons. Single and double asterisks indicate $P<0.05$ and $P<0.01$, respectively.

References
Banz, V. M., Medová, M., Keogh, A., Furer, C., Zimmer, Y., Candinas, D. and Stroka, D. (2009). Hsp90 transcriptionally and post-translationally regulates the expression of NDRG1 and maintains the stability of its modifying kinase GSK3beta. *Biochim. Biophys. Acta* 1793, 1597-1603. doi:10.1016/j.bbamcr.2009.08.002

Benitez, M. J., Sanchez-Ponce, D., Garrido, J. J. and Wandosell, F. (2014). Hsp90 activity is necessary to acquire a proper neuronal polarization. *Biochim. Biophys. Acta* 1843, 245-252. doi:10.1016/j.bbamcr.2013.11.013

Bounoutas, A., Kratz, J., Emtage, L., Ma, C., Nguyen, K. C. and Chalfie, M. (2011). Microtubule depolymerization in Caenorhabditis elegans touch receptor neurons reduces gene expression through a p38 MAPK pathway. *Proc. Natl. Acad. Sci. USA* 108, 3982-3987. doi:10.1073/pnas.1101360108

Bounoutas, A., O'Hagan, R. and Chalfie, M. (2009a). The multipurpose 15-protofilament microtubules in C. elegans have specific roles in mechanosensation. *Curr. Biol.* 19, 1362-1367. doi:10.1016/j.cub.2009.06.036

Bounoutas, A., Zheng, Q., Nonet, M. L. and Chalfie, M. (2009b). mec-15 encodes an F-box protein required for touch receptor neuron mechanosensation, synapse formation and development. *Genetics* 183, 607-617. doi:10.1534/genetics.109.105726

Brenner, S. (1974). The genetics of Caenorhabditis elegans. *Genetics* 77, 71-94.

Buchberger, A., Bukau, B. and Sommer, T. (2010). Protein quality control in the cytosol and the endoplasmic reticulum: brothers in arms. *Mol. Cell* 40, 238-252. doi:10.1016/j.molcel.2010.10.001

Chalfie, M. and Au, M. (1989). Genetic control of differentiation of the Caenorhabditis elegans touch receptor neurons. *Science* 243, 1027-1033. doi:10.1126/science.2646709

Cheng, P. L., Lu, H., Shelly, M., Gao, H. and Poo, M. M. (2011). Phosphorylation of E3 ligase Smurf1 switches its substrate preference in support of axon development. *Neuron* 69, 231-243. doi:10.1016/j.neuron.2010.12.021

Ciechanover, A. and Kwon, Y. T. (2017). Protein quality control by molecular chaperones in neurodegeneration. *Front. Neurosci.* 11, 185. doi:10.3389/fnins.2017.00185

D'Souza, S. M. and Brown, I. R. (1998). Constitutive expression of heat shock proteins Hsp90, Hsc70, Hsp70 and Hsp60 in neural and non-neural tissues of the rat during postnatal development. *Cell Stress Chaperones* 3, 188-199. doi:10.1379/1466-1268(1998)003<0188:CEOHSP>2.3.CO;2

Fraser, A. G., Kamath, R. S., Zipperlen, P., Martinez-Campos, M., Sohrmann, M. and Ahringer, J. (2000). Functional genomic analysis of C. elegans chromosome I by systematic RNA interference. Nature 408, 325-330. doi:10.1038/35042517

Gillan, V., Maitland, K., McCormack, G., Him, N. A. and Devaney, E. (2009). Functional genomics of hsp-90 in parasitic and free-living nematodes. Int. J. Parasitol. 39, 1071-1081. doi:10.1016/j.ijpara.2009.02.024

Hall, D. H. (1995). Electron microscopy and three-dimensional image reconstruction. Methods Cell Biol. 48, 395-436. doi:10.1016/S0091-679X(08)61397-7

Hartl, F. U., Bracher, A. and Hayer-Hartl, M. (2011). Molecular chaperones in protein folding and proteostasis. Nature 475, 324-332. doi:10.1038/nature10317

Hsu, J.-M., Chen, C.-H., Chen, Y.-C., McDonald, K. L., Gurling, M., Lee, A., Garriga, G. and Pan, C.-L. (2014). Genetic analysis of a novel tubulin mutation that redirects synaptic vesicle targeting and causes neurite degeneration in C. elegans. PLoS Genet 10, e1004715. doi:10.1371/journal.pgen.1004715

Ishimoto, T., Kamei, A., Koyanagi, S., Nishide, N., Uyeda, A., Kasai, M. and Taguchi, T. (1998). HSP90 has neurite-promoting activity in vitro for telencephalic and spinal neurons of chick embryos. Biochem. Biophys. Res. Commun. 253, 283-287. doi:10.1006/bbrc.1998.9701

Karney-Grobe, S., Russo, A., Frey, E., Milbrandt, J. and DiAntonio, A. (2018). HSP90 is a chaperone for DLK and is required for axon injury signaling. Proc. Natl. Acad. Sci. USA 115, E9899-E9908. doi:10.1073/pnas.1805351115

Kim, Y. T., Hur, E. M., Snider, W. D. and Zhou, F. Q. (2011). Role of GSK3 signaling in neuronal morphogenesis. Front. Mol. Neurosci. 4, 48. doi:10.3389/fnmol.2011.00048

Konishi, Y., Stegmuller, J., Matsuda, T., Bonni, S. and Bonni, A. (2004). Cdh1-APC controls axonal growth and patterning in the mammalian brain. Science 303, 1026-1030. doi:10.1126/science.1093712

Lindquist, S. and Craig, E. A. (1988). The heat-shock proteins. Annu. Rev. Genet. 22, 631-677. doi:10.1146/annurev.ge.22.120188.003215

Loones, M.-T., Chang, Y. H. and Morange, M. (2000). The distribution of heat shock proteins in the nervous system of the unstressed mouse embryo suggests a role in neuronal and non-neuronal differentiation. Cell Stress Chaperones 5, 291-305. doi:10.1379/1466-1268(2000)005<0291:TDOHSP>2.0.CO;2

Mello, C. and Fire, A. (1995). DNA transformation. Methods Cell Biol. 48, 451-482. doi:10.1016/S0091-679X(08)61399-0

Miller, D. J. and Fort, P. E. (2018). Heat shock proteins regulatory role in neurodevelopment. Front. Neurosci. 12, 821. doi:10.3389/fnins.2018.00821

Nakata, K., Abrams, B., Grill, B., Goncharov, A., Huang, X., Chisholm, A. D. and Jin, Y. (2005). Regulation of a DLK-1 and p38 MAP kinase pathway by the ubiquitin ligase RPM-1 is required for presynaptic development. Cell 120, 407-420. doi:10.1016/j.cell.2004.12.017

Quintá, H. R. and Galigniana, M. D. (2012). The neuroregenerative mechanism mediated by the Hsp90-binding immunophilin FKBP52 resembles the early steps of neuronal differentiation. Br. J. Pharmacol. 166, 637-649. doi:10.1111/j.1476-5381.2011.01783.x

Richie, C. T., Bembenek, J. N., Chestnut, B., Furuta, T., Schumacher, J. M., Wallenfang, M. and Golden, A. (2011). Protein phosphatase 5 is a negative regulator of separase function during cortical granule exocytosis in C. elegans. J. Cell Sci. 124, 2903-2913. doi:10.1242/jcs.073379

Röhl, A., Tippel, F., Bender, E., Schmid, A. B., Richter, K., Madl, T. and Buchner, J. (2015). Hop/Sti1 phosphorylation inhibits its co-chaperone function. EMBO Rep. 16, 240-249. doi:10.15252/embr.201439198

Sato, S., Fujita, N. and Tsuruo, T. (2000). Modulation of Akt kinase activity by binding to Hsp90. Proc. Natl. Acad. Sci. USA 97, 10832-10837. doi:10.1073/pnas.170276797

Schaefer, A. M., Hadwiger, G. D. and Nonet, M. L. (2000). rpm-1, a conserved neuronal gene that regulates targeting and synaptogenesis in C. elegans. Neuron 26, 345-356. doi:10.1016/S0896-6273(00)81168-X

Schmid, A. B., Lagleder, S., Gräwert, M. A., Röhl, A., Hagn, F., Wandinger, S. K., Cox, M. B., Demmer, O., Richter, K., Groll, M. et al. (2012). The architecture of functional modules in the Hsp90 co-chaperone Sti1/Hop. EMBO J. 31, 1506-1517. doi:10.1038/emboj.2011.472

Schwamborn, J. C., Müller, M., Becker, A. H. M. and Puschel, A. W. (2007). Ubiquitination of the GTPase Rap1B by the ubiquitin ligase Smurf2 is required for the establishment of neuronal polarity. EMBO J. 26, 1410-1422. doi:10.1038/sj.emboj.7601580

Singh, V. and Aballay, A. (2006). Heat-shock transcription factor (HSF)-1 pathway required for Caenorhabditis elegans immunity. Proc. Natl. Acad. Sci. USA 103, 13092-13097. doi:10.1073/pnas.0604050103

Song, H. O., Lee, W., An, K., Lee, H. S., Cho, J. H., Park, Z. Y. and Ahnn, J. (2009). C. elegans STI-1, the homolog of Sti1/Hop, is involved in aging and stress response. J. Mol. Biol. 390, 604-617. doi:10.1016/j.jmb.2009.05.035

Sulston, J. E., Schierenberg, E., White, J. G. and Thomson, J. N. (1983). The embryonic cell lineage of the nematode Caenorhabditis elegans. Dev. Biol. 100, 64-119. doi:10.1016/0012-1606(83)90201-4

Sun, Y., Hu, Z., Goeb, Y. and Dreier, L. (2013). The F-box protein MEC-15 (FBXW9) promotes synaptic transmission in GABAergic motor neurons in C. elegans. PLoS ONE 8, e59132. doi:10.1371/journal.pone.0059132

Tang, N. H. and Chisholm, A. D. (2016). Regulation of microtubule dynamics in axon regeneration: insights from C. elegans. F1000Res 5, 764. doi:10.12688/f1000research.8197.1

Tedeschi, A. and Bradke, F. (2013). The DLK signalling pathway–a double-edged sword in neural development and regeneration. EMBO Rep. 14, 605-614. doi:10.1038/embor.2013.64

Tuoc, T. C. and Stoykova, A. (2010). Roles of the ubiquitin-proteosome system in neurogenesis. Cell Cycle 9, 3174-3180. doi:10.4161/cc.9.16.12551

Uchida, S., Hara, K., Kobayashi, A., Fujimoto, M., Otsuki, K., Yamagata, H., Hobara, T., Abe, N., Higuchi, F., Shibata, T. et al. (2011). Impaired hippocampal spinogenesis and neurogenesis and altered affective behavior in mice lacking heat shock factor 1. Proc. Natl. Acad. Sci. USA 108, 1681-1686. doi:10.1073/pnas.1016424108

Vaughan, C. K., Mollapour, M., Smith, J. R., Truman, A., Hu, B., Good, V. M., Panaretou, B., Neckers, L., Clarke, P. A., Workman, P. et al. (2008). Hsp90-dependent activation of protein kinases is regulated by chaperone-targeted dephosphorylation of Cdc37. Mol. Cell 31, 886-895. doi:10.1016/j.molcel.2008.07.021

Wandinger, S. K., Suhre, M. H., Wegele, H. and Buchner, J. (2006). The phosphatase Ppt1 is a dedicated regulator of the molecular chaperone Hsp90. EMBO J. 25, 367-376. doi:10.1038/sj.emboj.7600930

Wang, Z., Hou, Y., Guo, X., van der Voet, M., Boxem, M., Dixon, J. E., Chisholm, A. D. and Jin, Y. (2013). The EBAX-type Cullin-RING E3 ligase and Hsp90 guard the protein quality of the SAX-3/Robo receptor in developing neurons. Neuron 79, 903-916. doi:10.1016/j.neuron.2013.06.035

Watkins, T. A., Wang, B., Huntwork-Rodriguez, S., Yang, J., Jiang, Z., Eastham-Anderson, J., Modrusan, Z., Kaminker, J. S., Tessier-Lavigne, M. and Lewcock, J. W. (2013). DLK initiates a transcriptional program that couples apoptotic and regenerative responses to axonal injury. Proc. Natl. Acad. Sci. USA 110, 4039-4044. doi:10.1073/pnas.1211074110

Wayne, N., Mishra, P. and Bolon, D. N. (2011). Hsp90 and client protein maturation. Methods Mol. Biol. 787, 33-44. doi:10.1007/978-1-61779-295-3_3

Yamada, T., Yang, Y. and Bonni, A. (2013). Spatial organization of ubiquitin ligase pathways orchestrates neuronal connectivity. Trends Neurosci. 36, 218-226. doi:10.1016/j.tins.2012.12.004

Yan, D. and Jin, Y. (2012). Regulation of DLK-1 kinase activity by calcium-mediated dissociation from an inhibitory isoform. Neuron 76, 534-548. doi:10.1016/j.neuron.2012.08.043

Yan, D., Wu, Z., Chisholm, A. D. and Jin, Y. (2009). The DLK-1 kinase promotes mRNA stability and local translation in C. elegans synapses and axon regeneration. Cell 138, 1005-1018. doi:10.1016/j.cell.2009.06.023

Zheng, C., Diaz-Cuadros, M. and Chalfie, M. (2015). Dishevelled attenuates the repelling activity of Wnt signaling during neurite outgrowth in Caenorhabditis elegans. Proc. Natl. Acad. Sci. USA 112, 13243-13248. doi:10.1073/pnas.1518686112

Zheng, C., Diaz-Cuadros, M., Nguyen, K. C. Q., Hall, D. H. and Chalfie, M. (2017). Distinct effects of tubulin isotype mutations on neurite growth in Caenorhabditis elegans. Mol. Biol. Cell 28, 2786-2801. doi:10.1091/mbc.e17-06-0424

Zheng, C., Jin, F. Q., Trippe, B. L., Wu, J. and Chalfie, M. (2018). Inhibition of cell fate repressors secures the differentiation of the touch receptor neurons of Caenorhabditis elegans. Development 145, dev168096. doi:10.1242/dev.168096

Gene name	Allele name	Molecular lesion	Recessivity	Maternal effect
sti-1	*u1071*	R253*	recessive	Yes
pph-5	*u1072*	C381Y	recessive	Yes
pph-5	*u1073*	P448L	recessive	Yes
pph-5	*u1074*	Q325*	recessive	Yes
pph-5	*u1075*	Q192*	recessive	Yes
dlk-1	*u1105*	V844I	recessive	Yes
dlk-1	*u1138*	W394*	recessive	Yes
maph-1.3	*u1107*	E794K	dominant	N/A
?	*u1108*		dominant	N/A
?	*u1106*		semi-dominant	N/A
?	*u1142*		semi-dominant	N/A
?	*u1144*		semi-dominant	N/A

Table S1. Summary of the mutants isolated from the *mec-15(-)* suppressor screen. These alleles led to the production of a long ALM-PN in *mec-15(u1042); mec-7(u278); uIs115[mec-17p::TagRFP]* animals. * represents a stop codon; ? means the mutant allele was not mapped.

Gene name	Transcript name	Description	Long ALM-PN
pph-5	Y39B6A.2	Protein Phosphatase 5	Positive
sti-1	R09E12.3	Hsp90 co-chaperone; Hop/STI1	Positive
hsp-1	F26D10.3	Hsp70 family	Negative
hsp-110	C30C11.4	HSPA4; Hsp70 family	Positive
hsp-3	C15H9.6	HSPA5; Hsp70 family	Negative
hsp-4	F43E2.8	HSPA5; Hsp70 family	Negative
hsp-6	C37H5.8	HSPA9; Hsp70 family	Negative
stc-1	F54C9.2	HSPA13; Hsp70 family	Negative
hsp-70	C12C8.1	Hsp70 family	Negative
F44E5.4	F44E5.4	Hsp70 family	Negative
F44E5.5	F44E5.5	Hsp70 family	Negative
T14G8.3	T14G8.3	HYOU1; Hsp70 family	Negative
hsp-75	R151.7	Hsp90-related protein; Hsp75/TRAP1	Negative
enpl-1	T05E11.3	Molecular Chaperone; GRP94/GP96	Negative
chn-1	T09B4.10	CHIP; Hsp70-interacting protein	Negative
daf-41	ZC395.10	Hsp90 co-chaperone; p23	Positive
aha-1	C25A1.11	Hsp90 co-chaperone; Aha1	Negative
aipr-1	C56C10.10	Hsp90 co-chaperone; XAP2	Negative
bag-1	F57B10.11	Hsp90 co-chaperone; Bag-1	Negative
fkb-6	F31D4.3	FK506-Binding protein; Hsp90-interacting protein	Negative
cdc-37	W08F4.8	Hsp90 co-chaperone; cdc37	Negative
trak-1	T27A3.1	HAP1; Hsp90-interacting protein	Negative
tomm-70	ZK370.8	TPR repeat-containing mitochondrial protein	Negative
sgt-1	R05F9.10	PPH-5 homolog; TRP repeat-containing protein	Negative
cct-1	T05C12.7	Chaperonin Containing TCP-1	Negative
hsb-1	K08E7.2	Heat shock factor binding protein	Negative
lit-1	W06F12.1	Serine/threonine-protein kinase NLK	Negative

Table S2. Results of the candidate RNAi screen for *mec-15(-)* suppressors. *mec-15(u75); eri-1(mg366) uIs115; mec-7(u278) lin-15B(n744)* animals were fed with RNAi bacteria. If 10% of the treated animals had ALM-PN longer than five cell body length, the treatment was considered to produce positive results.
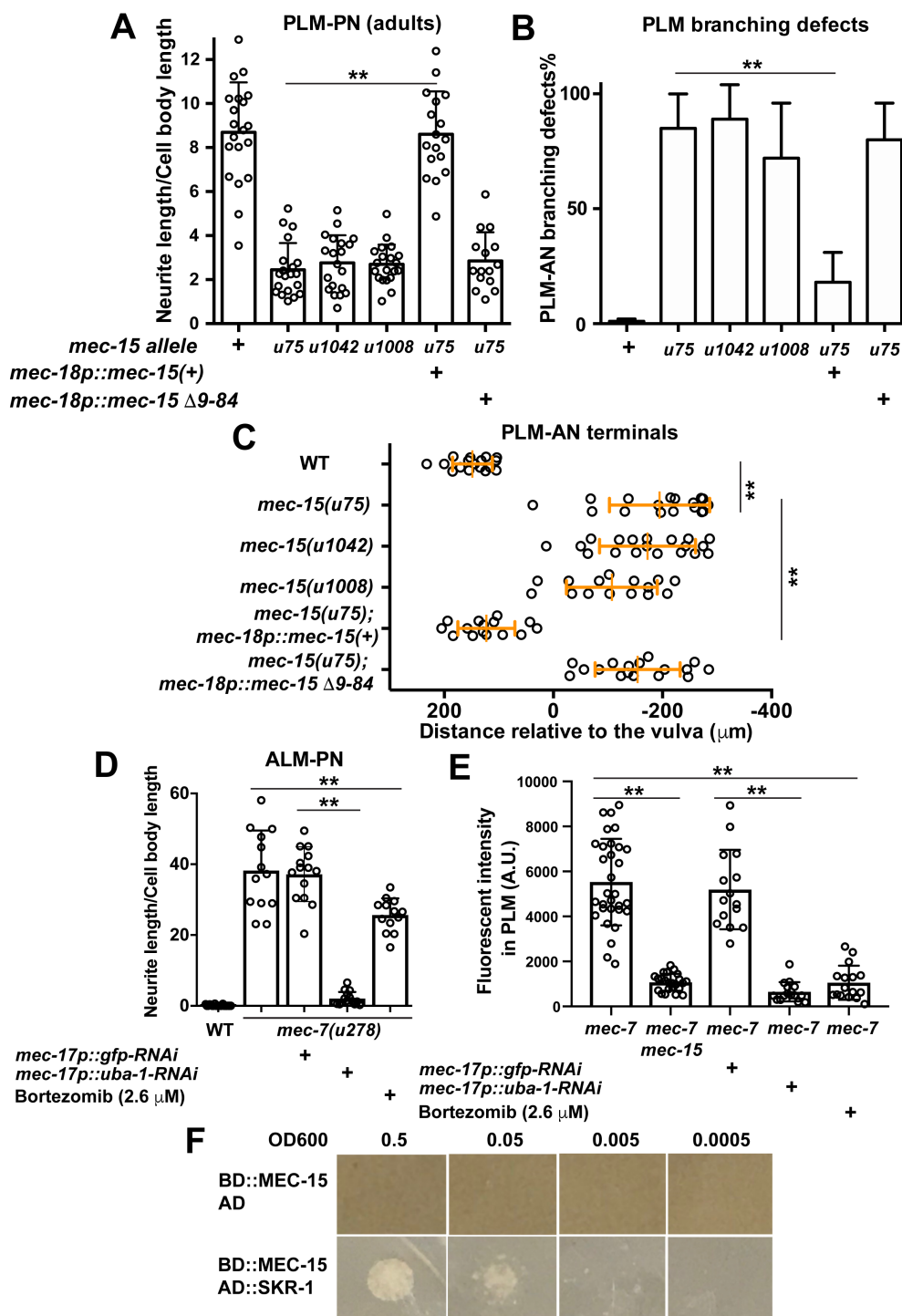
Figure S1. F-box protein MEC-15 is required for TRN neurite development. (A) The length of

PLM-PN in animals carrying various *mec-15 lf* alleles and *mec-15(u75)* mutants carrying the transgene

expressing either wild-type MEC-15 (+) or MEC-15 Δ9-84 truncates from the TRN-specific *mec-18*

promoter. (B) The percentage of PLM cells with PLM-AN branching defects in various strains. N > 40.

(C) The distance of PLM-AN terminals to the vulva in the indicated strains. The distance is positive if

PLM-AN grew pass the vulva towards the anterior and negative if PLM-AN did not reach the vulva.

(D) The length of ALM-PN in wild type (WT), *mec-7(u278)* mutants, and *mec-7* animals carrying the transgene expressing dsRNA against *uba-1* from the TRN-specific *mec-17* promoter, as well as in *mec-7* animals grown on plates containing 2.6 μM bortezomib. (E) TagRFP fluorescent intensity in PLM neurons of *mec-7(u278)* mutants, *mec-7 mec-15(u1042)* double mutants, and *mec-7* animals with *uba-1* knockdown or bortezomib treatment. (F) Yeast two-hybrid assays for the interaction between MEC-15 and SKR-1. AD means the GAL4 activation domain and BD means the GAL4 DNA-binding domain.
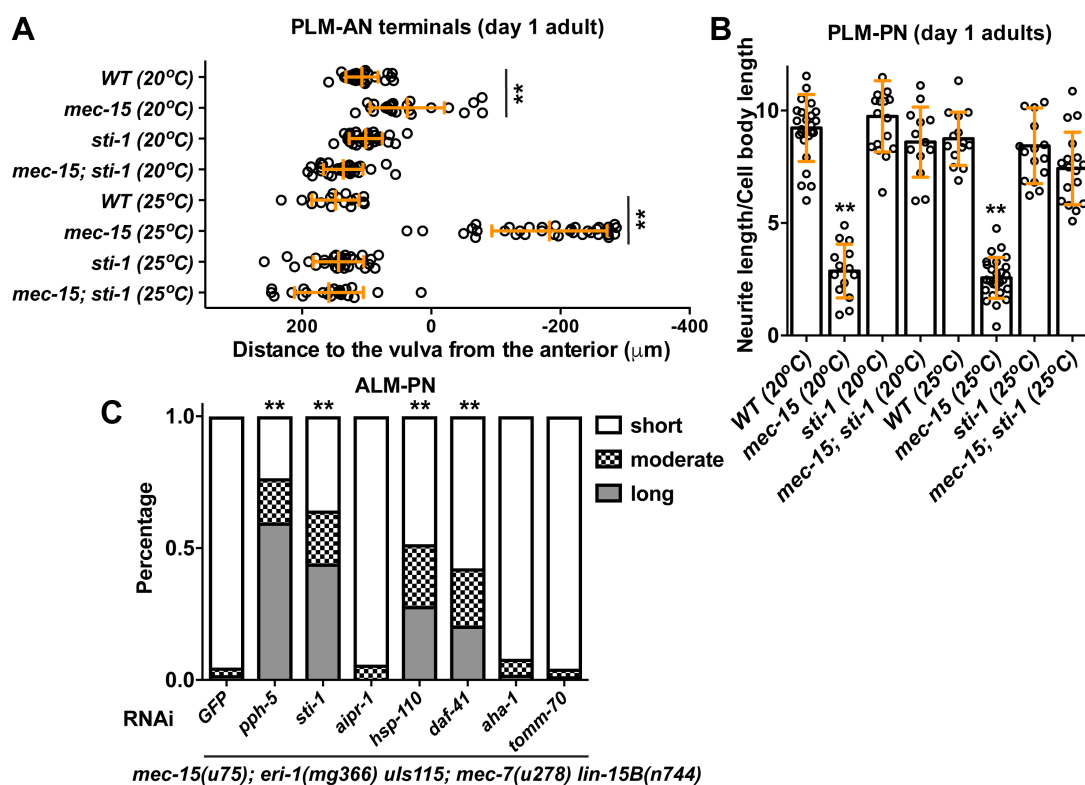
Figure S2. Mutations or knockdown of Hsp90 cochaperones suppress the phenotype of *mec-15* mutants. (A) The distance of PLM-AN terminals to the vulva in wild type (WT) *mec-15(u1042), sti-1(ok3354)* and *mec-15; sti-1* animals at both 20 and 25 °C. (B) The length of PLM-PN in *mec-15(u1042), sti-1(ok3354)* and *mec-15; sti-1* animals at both 20 and 25 °C. Double asterisks indicate statistical significance ($p < 0.01$) for the difference between *mec-15* mutants and the wild type animals. (C) The percentage of ALM cells with short (< 2 cell body length), moderate (2-5 cell body length), or long (> 5 cell body length) ALM-PN in *mec-15; eri-1 uIs115[mec-17p::TagRFP]; mec-7 lin-15B;* animals fed with bacteria that express dsRNA against the genes indicated. Double asterisks indicate statistical significance ($p < 0.01$) for the difference between the treatment and the RNAi against GFP in a Chi-square test.
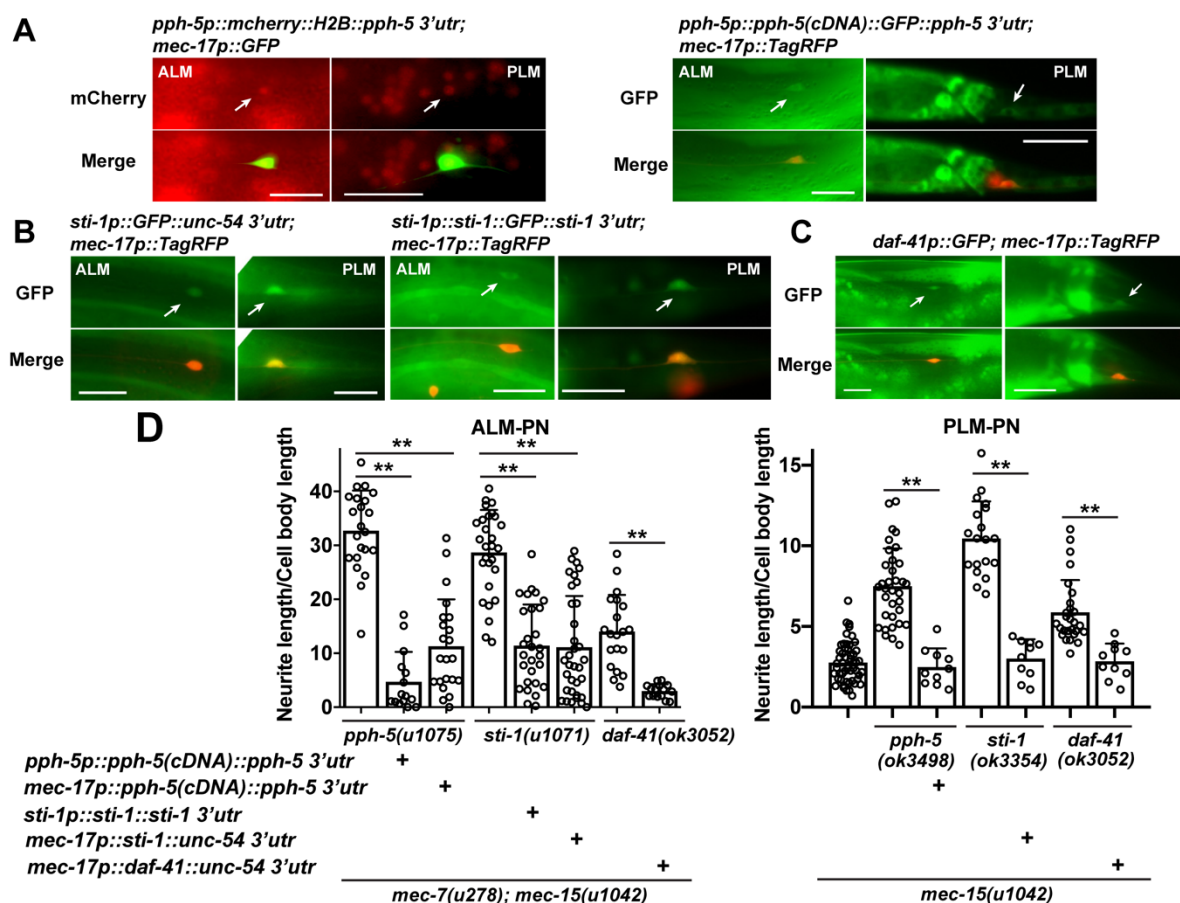
Figure S3. Hsp90 cochaperones are expressed in the TRNs and function cell-autonomously. (A) The expression of *pph-5* transcriptional reporter *avIs90[pph-5p::mCherry::H2B::pph-5 3'utr; unc-119(+)]* (Richie et al., 2011) and translational reporter *unkEx36[pph-5p::pph-5_cDNA::GFP::pph-5 3'utr; unc-119(+)]* in TRNs. (B) The expression of *sti-1* transcriptional reporter *unkEx52[sti-1p::GFP::unc-54 3'utr]* and translational reporter *unkEx24[sti-1p::sti-1::GFP::sti-1 3'utr; unc-119(+)]* in TRNs. (C) The expression of *daf-41* transcriptional reporter *sEx10796[daf-41p::GFP]* in TRNs. Arrows point to the cell bodies of ALM and PLM. Scale bar = 20 μm. (D) The length of ALM-PN in the triple mutants that expressed the rescuing transgenes and the length of PLM-PN in the double mutants that expressed the transgenes. Double asterisks indicate statistical significance ($p < 0.01$).
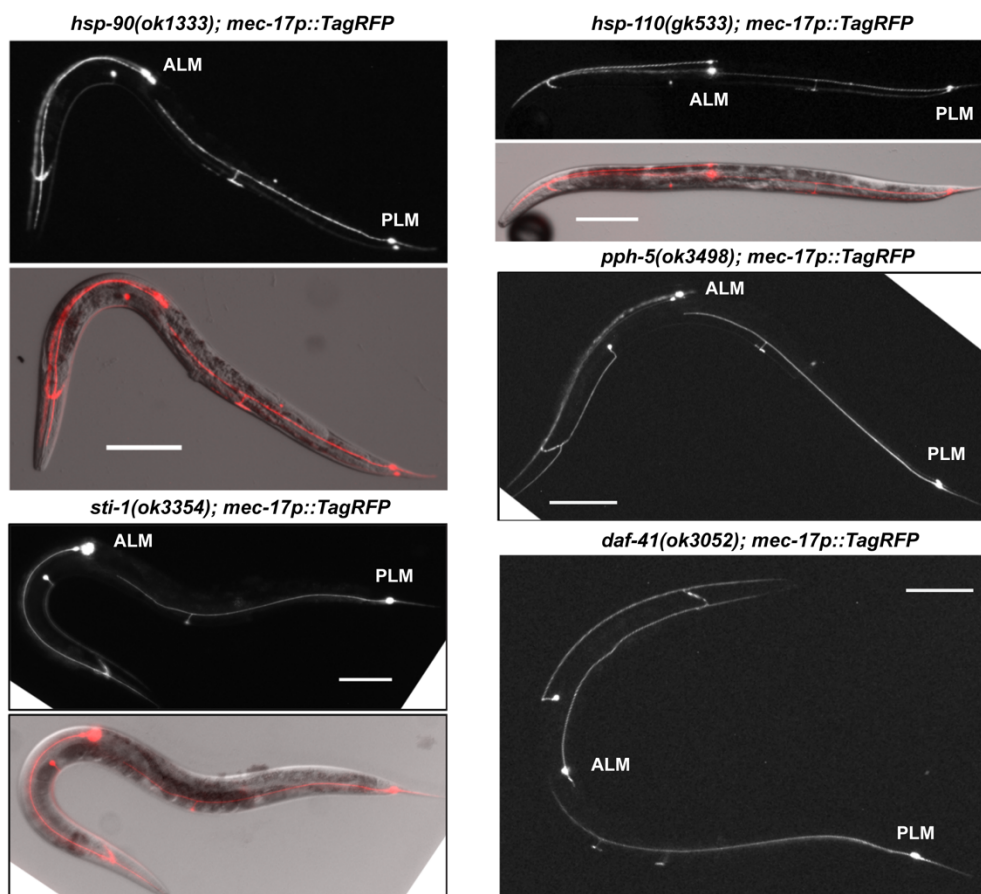
Figure S4. Single mutants of Hsp70/90 chaperones and cochaperones showed normal TRN morphologies. TRN morphologies were visualized by the *mec-17p::TagRFP* transgene in *hsp-90*, *hsp-110*, *sti-1*, *pph-5*, and *daf-41* mutants. *hsp-90* and *hsp-110* homozygotes were the progeny of the balanced heterozygotes *hsp-90/nT1* and *hsp-110/hT2*, respectively. Scale bars = 100 μm.
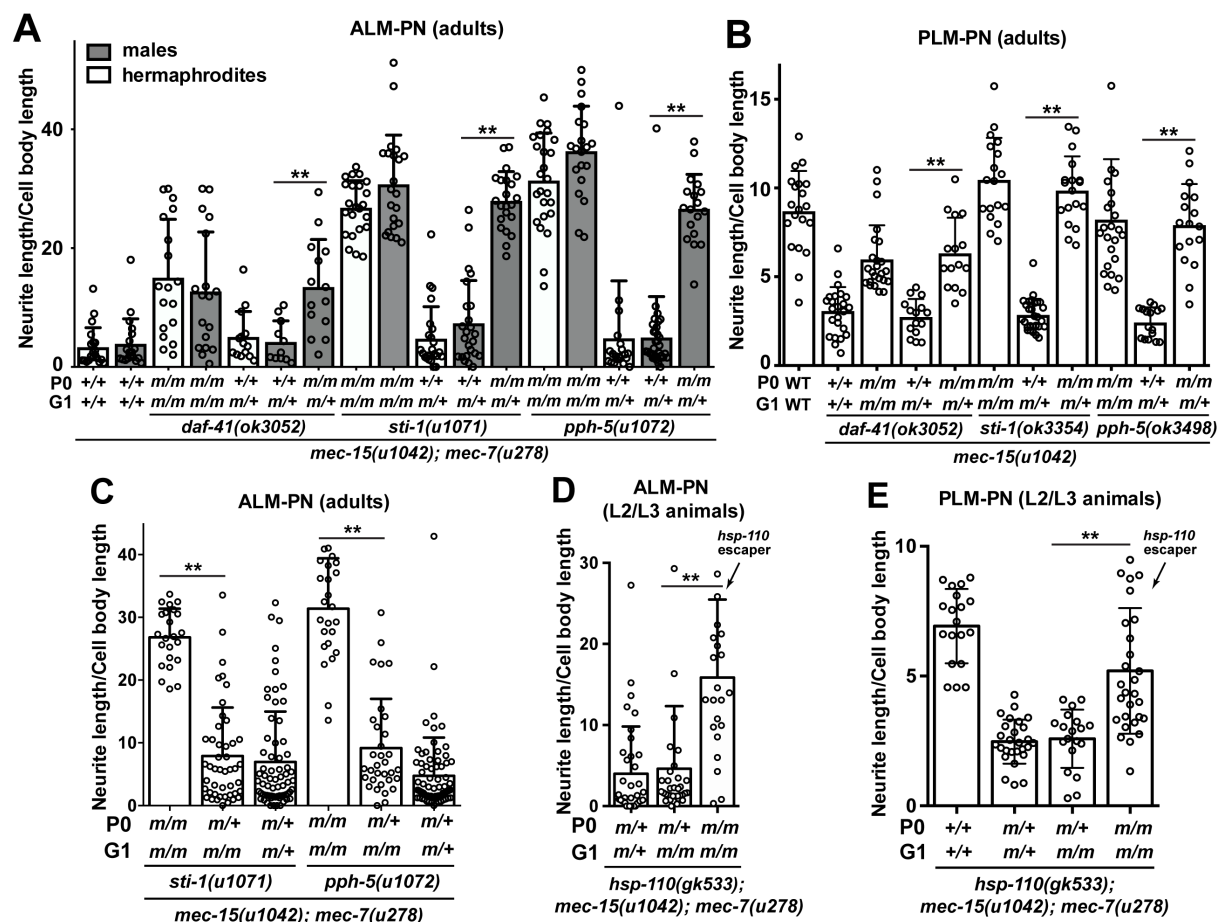
Figure S5. Maternal effects of Hsp70/Hsp90 chaperone and cochaperone mutants. (A) The length of ALM-PN of the heterozygous cross-progeny between *mec-15; mec-7* double mutants and their triple mutants with *daf-41*, *sti-1*, or *pph-5 lf* mutations. P0 indicates the genotype of the mother of the animals (G1 for generation 1) that were examined; "m" represents the mutant allele and "+" the wild-type allele. Crosses to generate heterozygous progeny were repeated three times. (B) The length of PLM-PN of the heterozygous cross-progeny between *mec-15* single mutants and the *mec-15* double mutants with *daf-41*, *sti-1*, or *pph-5 lf* mutations. (C-D) The length of ALM-PN of the self-progeny of *sti-1/+; mec-15; mec-7* and *pph-5/+; mec-15; mec-7* animals and the progeny of *hsp-110/+; mec-15; mec-7* hermaphrodites and the *hsp-110; mec-15; mec-7* escapers. (E) The length of PLM-PN of the self-progeny of *hsp-110/+; mec-15;* hermaphrodites and the *hsp-110; mec-15* escapers. *hsp-110* homozygotes mostly arrested at larval stages.
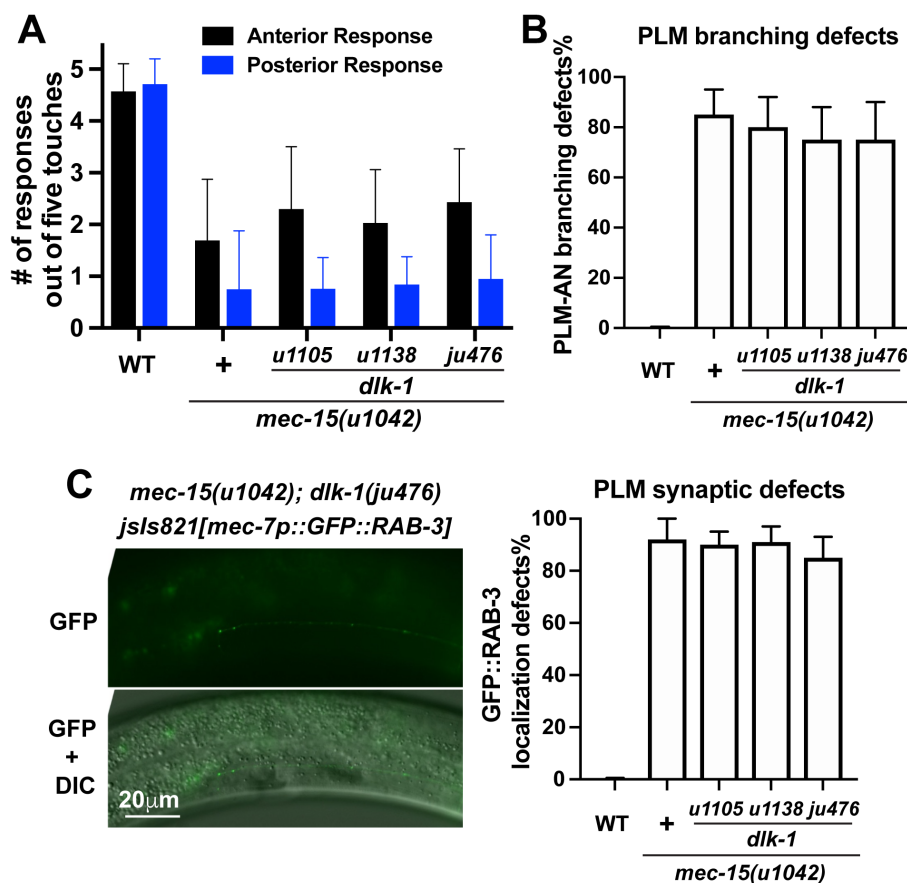
Figure S6. Mutations in *dlk-1* fail to rescue the defects in TRN synaptic development and sensory function of *mec-15* mutants. (A) The number of gentle touch response out of five stimuli in *mec-15* and *mec-15 dlk-1* mutants. (B) The percentages of PLM cells with PLM-AN branching defects in *mec-15* and *mec-15 dlk-1* mutants. (C) Defects of synaptic vesicle (GFP::RAB-3) localization in *mec-15 dlk-1* mutants. The percentage of PLM cells with abnormal GFP::RAB-3 localization in *mec-15* and *mec-15 dlk-1* mutants.
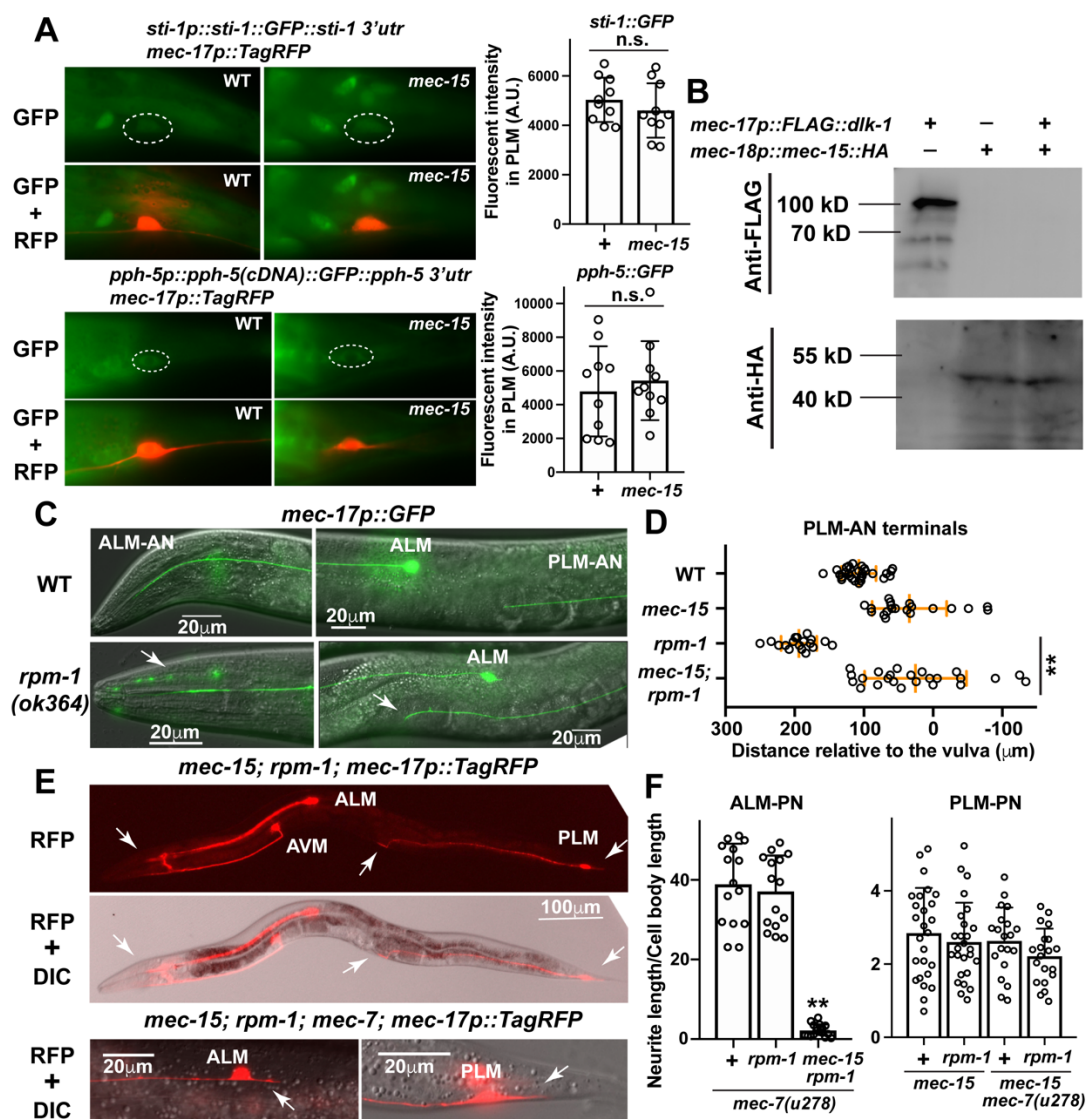
Figure S7. MEC-15 downregulates DLK-1 and is epistatic to RPM-1. (A) Fluorescence of STI-1::GFP and PPH-5::GFP in PLMs of the wild-type and *mec-15(u1042)* animals. Dashed circles enclosed the PLM cell bodies. Quantification of the GFP fluorescent intensity in PLM cells are shown. (B) Western blot with anti-FLAG or anti-HA antibodies with animals carrying transgenes expressing either FLAG::DLK-1 or MEC-15::HA or both in TRNs. (C) Overextension of ALM-AN and PLM-AN in *rpm-1(ok364)* mutants. (D) The distance of PLM-AN terminals to the vulva in *mec-15(u1042)*, *rpm-1(ok364)*, and *mec-15; rpm-1* mutant animals. (E) The shortening of ALM-AN, PLM-AN, and PLM-PN in *mec-15; rpm-1* mutant and the shortening of ALM-PN and PLM-PN in *mec-15; rpm-1; mec-7* animals. Arrows indicate the shortened neurites. (F) The length of ALM-N and PLM-PN in various strains indicated. Double asterisks indicate statistical significance ($p < 0.01$) for the difference between *rpm-1* and *mec-15; rpm-1* mutants.